UDC 533.6.071.4 :
533.6.011.3

TECHNICAL REPORT OF NATIONAL AEROSPACE LABORATORY

TR-252T

A Study of Subsonic, Two-Dimensional Wall-Interference Effect in a Perforated Wind Tunnel with Particular Rererence to the NAL 2m×2m Transonic Wind Tunnel—Inapplicability of the Conventional Boundary Condition

Masao EBIHARA

January 1972

NATIONAL AEROSPACE LABORATORY

CHŌFU, TOKYO, JAPAN

List of NAL Technical Reports

TR-231 Two-Dimensional Cascade Test of an Air-Cooled Turbine Nozzle. (Part I On the Experimental Results of a Convection-Cooled Blade)	Toyoaki YOSHIDA, Kitao TAKAHARA, Hiroyuki NOUSE, Shigeo INOUE, Fujio MIMURA & Hiroshi USUI	Jan. 1971
TR-232 Two-Dimensional Cascade Test of an Air-Cooled Turbine Nozzle (Part II On the Temperature Distributions of a Convection-Cooled Blade by Numerical Calculation and Analogue Simulation Test)	Toyoaki YOSHIDA, Kitao TAKAHARA, Hiroyuki NOUSE, Shigeo INOUE, Fujio MIMURA & Hiroshi Usui	Jan. 1971
TR-233 Studies on PSD Method to Aircraft Structural Design for Atmospheric Turbulence	Kazuyuki TAKEUCHI, Kozaburo YAMANE	Jan. 1971
TR-234 A Calculation of Temperature Distribution with Applying Green Function to Two-Dimensional Laplaces Equation	Hideaki NISHIMURA	Jan. 1971
TR-235 Preliminary Experiments for Automatic Landing. (1) On the Performance Tests of Radio Altimeters	Kazuo HIGUCHI, Yuso HORIKAWA, Mikihiko MORI, Koichi OGAWA, Mitsuyoshi MAYANAGI, Akira WATANABE & Takayuki NAGOSHI	Apr. 1971
TR-236 T Small-Strain Deformations Superposed on Finite Deformations of Highly Elastic Incompressible Meterials, Part I—Constitutive Equation	Tastuzo KOGA	Jun. 1971
TR-237 Free Flight Tests on Longitudinal Dynamics Characteristics of FFM-10 Model	Toshio KAWASAKI, Taketoshi HANAWA, Hideo SAITO, Kazuaki TAKASHIMA & Iwao KAWAMOTO	Apr. 1971
TR-238 Dynamic Characteristic of Lift Jet Engine JR 100H	Kenji NISHIO, Masanori ENDO, Nanahisa SUGIYAMA, Takeshi KOSHINUMA & Toshimi OHATA	May. 1971
TR-239 A Direct Calculation of Subliming Ablation	Hirotoshi KUBOTA	Jun. 1971
TR-240 T A Method for the Calculation of Lifting Potential Flow Problems —Part I— Theoretical Basis	Masao EBIHARA	July 1971
TR-241 Full-Scale Fatigue Test of YS-11A-500/600 Turboprop Transport Wing (I Safe life Fatigue Test Loads and Test Method)	Kazuyuki TAKEUCHI, Toshio NOHARA & Hiroo ASADA	July 1971
TR-242 Measurement of three-dimensional mean Velocity Vector and Reynolds Stress by Single Rotatable Hot-wire	Yoshio HAYASHI, Teruomi NAKAYA	July 1971
TR-243 A Method for the Calculation of Lifting Potential Flow Problems —Part 1— Theorotical Basis	Masao EBIHARA	July 1971
TR-244 Measurements of Dynamic Stability Derivatives in Supersonic Blowdown Wind Tunnel	Kazuaki TAKASHIMA, Seizo SAKAKIBARA & Hideo SEKINE	July 1971
TR-245 An Analytical Method to Predict Height-Velocity Diagram Critical Decision Point of Rotorcraft	Masaki KOMODA	Aug. 1971
TR-246 On Analysis of Large Deformation Problems of Beam	Hideo Izumi	Nov. 1971

A Study of Subsonic, Two-Dimensional Wall-Interference Effects in a Perforated Wind Tunnel with Particular Reference to the NAL 2 m×2 m Transonic Wind Tunnel—Inapplicability of the Conventional Boundary Condition*

By Masao EBIHARA**

SUMMARY

An analysis is carried out on the subsonic, two-dimensional wall-interference effects in a perforated wind tunnel based on the conventional theoretical model. An attempt is then made to find the value of the porosity parameter for the 20%-open-area-ratio test section of the NAL 2 m×2 m transonic wind tunnel by combining the results of the analysis with pressure distribution data on several aerofoil models obtained using this test section.

It is found that no meaningful results can be achieved by this procedure for the value of the porosity parameter. The cause of the failure is ascribed to the inappropriateness of the boundary condition in the theoretical model employed. An alternative form of the boundary condition is suggested based on experimental observations of flow in the proximity of perforated boundaries.

I. INTRODUCTION

The pressure distribution on an aerofoil measured in a wind tunnel is in general subject to a distortion due to the tunnel-wall interference effects. These interference effects must be known accurately when the experimental data are to be relied upon to estimate the performance of an aerofoil at the free-air condition or to assess the accuracy of a theoretical method for the prediction of the pressure distribution on an aerofoil.

The aerofoil theory has arrived at a stage where a detailed prediction of the pressure distribution on an aerofoil is feasible at Mach numbers below the critical with accuracy sufficient for most of the practical purposes (e.g. refs. 1 & 2). The prediction, of course, takes into account not only the effects of compressibility but also the effects of viscosity by modifying the aerofoil geometry according to the displacement effects of the boundary layer. It is known that these displacement effects exert influences on the pressure distribution usually at least of the same order of magnitude as the second-order compressibility effects. On the other hand, the wall-interference effects are found to be by an order of magnitude greater than the boundary layer effects in the 20%-open perforated-wall test section of our 2m×2m wind tunnel, which is thought to be representative of transonic wind tunnels of this kind. Thus it is recognized that a detailed analysis is required of the wall-interference effects in order to bring the accuracy of the prediction method to a level comparable with that in the prediction of the boundary layer effects.

The principles for the calculation of the wall-interference effects have long been established within the scope of the linearized theory and numerous theoretical works already exist which dealt with the interference problems in wind tunnels with ventilated test sections such as of slotted and perforated walls. General description of the interference problems is found, e.g., in the work of Garner, Rogers, Acum and Maskell (ref. 3), or of Goe-

* Received 7th October, 1971

** The Second Aerodynamics Division.

thert (ref. 4). A summary of part of the existing theoretical works is given in Table I, where included are some of the reports appeared after the publication of the two comprehensive works referred to above. The methods listed in the Table are all based on the linearized theory and the analysis has been carried out, except those in refs. 8, 9 and 19, by replacing the body in the wind tunnel with concentrated singularities such as doublets and vortices. For each work listed, the kind of the singularity used to represent the body is given in the Table together with the mathematical procedures employed to solve the problem. The first part of the Table is concerned with the cases of perforated test sections whereas the second part lists the cases where the test sections are of longitudinally slotted walls. Mathematically, the two cases are discriminated from each other by the difference in the form of the boundary condition along the test-section wall. In fact, the two boundary conditions can be united by an appropriate linear combination and it is possible to solve the interference problem for this combined boundary condition. This approach yields results from which both the perforated-wall cases and the slotted-wall ones are derived as particular cases. The last part of the Table deals with the works which follow this approach.

Two problems emerge when one attempts to apply the theoretical results to the estimation of the interference effects upon the pressure distribution on an aerofoil measured in a wind tunnel of perforated test section. The first one is related to the accuracy of the existing theoretical methods in which it is customary to replace the aerofoil by a concentrated singularity like a doublet or vortex. This procedure may be adequate for cases where the interference effects on the overall forces and moments are of concern. It is probable, how-

Table I. Existing Theoretical Methods

1. Perforated-wall Tunnel

interference category / type of test-section	Solid Blockage	Lift Effects
Two-dimensional	(3)* ** WADC TR 52-9, 1952 (5) NACA TM 1429, 1957 (8) Proc. Roy. Soc. A. Vol. 233, 1955 thin aerofoil finite length of perforated portion of the wall variable plenum pressure tangent-gas method	(5) NACA TM 1429, 1957 (9) Proc. Roy. Soc. A. Vol 242, 1957 same as left
Rectangular, all walls perforated		(17), (18) NASA TR R-285, 1968 NASA TN D-5635, 1970 horseshoe vortex approximate method (by Fourier transformation) (15) Aeron. Quart. Vol. XIX, Pt. 4, 1968 vortex doublet along the tunnel axis dynamic relaxation method

* The number in parenthesis attached to each report name indicates the reference number listed at the end of the present report.

** Results reported in the paper are quoted in ref. 3. The original paper has not been consulted by the present author.

ever, that the streamwise extent of the aerofoil geometry may have appreciable influence upon the interference effects on the pressure distribution so that the representation of the aerofoil by a concentrated singularity may not be justified when one is concerned with the pressure distribution data. One way of improving this situation is to represent the aerofoil by a system of distributed singularities as has been done, for instance, by Woods (refs. 8 & 9) or by de Jager & van de Vooren (ref. 19).

The second problem is related to the fact that there is one aspect of indeterminancy in the boundary condition for the perforated test section. In the calculation of the wall-interference effects, usual practice is to replace the actual perforated wall by a fictitious boundary of homogeneous property which would produce the identical effect in the region of flow field near the body. Theoretical considerations suggest that this homogeneous boundary replacing the actual wall is such that the normal velocity through it is proportional to the pressure difference across it (e.g. refs. 20 & 21). The coefficient of proportionality, called the 'porosity parameter', cannot however be determined from mere theoretical considerations and recourse

Table I. Existing Theoretical Methods — continued
2. Slotted-wall Tunnel

type of test-section \ interference category		Solid Blockage	Lift Effects
Two-dimensional			(10) NASA TR R-25, 1959 vortex at arbitrary vertical position
Circular		(6) NACA RM L53E07b, 1953 sphere (doublet)	(6) NACA RM L53E07b, 1953 streamwise vortex pair (far downstream part of a horseshoe vortex) two-dimensional consideration in a cross-section far downstream
Rectangular	closed side walls	(6) NACA RM L53E07b, 1935 sphere (doublet)	(6) NACA RM L53E07b, 1953 streamwise vortex pair (10) NASA TR R-25, 1959 horseshoe vortex approximate procedure combining a two-dimensional consideration with a correction by an interpolation between open and closed-wall cases (11) NASA TR R-241, 1966 system of line doulets double Fourier transformation
	all walls slotted		(6) NACA RM L53E70b, 1953 streamwise vortex pair
	closed roof and floor		(12) NASA TR R-344, 1970 system of line doublets double Fourier transformation

must be made to experiments to find its value for a particular wind tunnel test section.

The purpose of the present investigation is thus two-fold:

(1) to derive an expression of the interference effects of a perforated-wall test section with accuracy such that it can be applied consistently to the correction of the pressure distribution data, and

(2) to find the value of the porosity parameter appropriate to the transonic test section of the NAL 2m×2m wind tunnel.

A solution for the first problem is undertaken in Section III by adopting an approach similar to that taken in ref. 19. But before launching that, the nature of the boundary condition for the perforated wall is reviewed in Section II in an attempt to clarify its implication and limitation as a representative of the actual situation. Then in Section IV, the theoretical results obtained in Section III are applied to the analysis of experimental data in order to derive the value of the porosity parameter relevant to the 20%-open-area-ratio test section of the NAL 2m×2m transonic wind tunnel from the measured pressure distributions on several aerofoil models.

NOMENCLATURE

c	aerofoil-chord length
c_1, c_2, c_3	constants related to the aerofoil geometry, see eq (3. 35)
H	height of the wind tunnel test section
K	coefficient in the boundary condition, see (2.5)
M_∞	free-stream Mach number
M_W	aerofoil first moment of area about the leading-edge, see eq. (3. 45 b)
P	porosity parameter, $=1/K$
q	strength of source
S_W	aerofoil sectional area, see eq. (3. 45a)
t	non-dimensional streamwise coordi-

Table I. Existing Theoretical Methods — concluded
3. Unified Treatments of Slotted-Perforated Tunnel

interference category / type of test-section		Solid Blockage	Lift Effects
Two-dimensional		(7) NACA TN 3176, 1954 circle (by doublet)	
Circular		(7) NACA TN 3176, 1954 sphere (by doublet) Fourier transformation	(7) NACA TN 3176, 1954 vortex doublet along the tunnel axis Fourier transformation
Rectangular	closed side walls		(13) A.R.C. R & M 3322, 1963 vortex doublet along the tunnel axis (14) A.R.C. R & M 3395, 1965 distributed vortex doublet, explicit expressions only for uniformly loaded wings (viz. a horseshoe vortex) Fourier transformation
	all walls ventilated		(16) A.R.C. R & M 3567, 1969 vortex doublet along the tunnel axis electrical analogue

nate, $=x/c$

u streamwise component of the disturbance velocity

U_∞ free-stream velocity

v component of the disturbance velocity normal to the tunnel centre-line

w complex potential

x, x_0 streamwise coordinate

y coordinate normal to the tunnel centre-line

y_c aerofoil camber

y_t aerofoil thickness distribution

α aerofoil incidence

β Prandtl-Glauert factor, $=\sqrt{1-M_\infty^2}$

γ strength of vortex

δ see eq. (2. 13)

ϵ_s solid blockage factor

ξ non-dimensional streamwise coordinate, $=x/c$

ξ_0 see eq. (3. 25 a)

ξ_1, ξ_2 see eq. (3. 13)

κ $=\delta/\pi$

λ aerofoil-chord-to-tunnel-height ratio, $=c/H$

τ $=\pi\lambda(\xi-t)$

φ disturbance velocity potential

Subscripts

∞ refers to the free-stream condition

0 refers to the free-air condition

1 refers to the interference effects

II. A REVIEW ON THE BOUNDARY CONDITION ALONG THE PERFORATED WALL

2. 1. The theoretical mean boundary condition

According to Maeder & Thommen (ref. 20), the flow near a perforated wall is classified into three categories as follows:

(1) when the holes of the perforated wall are very small, any flow through them will occur in accordance with the law of slow viscous motion. Such walls are properly classified as 'porous walls'.

(2) If the hole diameter is still small compared to the thickness of the wall boundary layer but large enough so that the cross-flow pressure loss due to viscous action is insignificant, then the disturbance from the individual holes will be averaged at some distance from the wall, still inside the boundary layer, and the flow there can be regarded mathematically as one caused by an imaginary mean boundary at the location of the actual wall.

(3) If the hole diameter is large compared to the boundary layer thickness at the wall, each hole has to be treated individually, considering the past history of the boundary layer flow.

In most of the existing perforated-wall wind tunnels, the configuration of the test-section wall is such that they fall on the category (2) stated above. The mean boundary condition for such walls has been deduced by several authors, one of the earliest derivations being due to Brescia (ref. 5). In the two-dimensional case, the perforated wall reduces to a series of transverse slots (or slats). Neglecting the thickness of the slats and taking them as a series of flat plates, Brescia argues that this cascade-like boundary induces a uniform streamwise velocity increment $\pm u_\infty$ at an infinite distance above and below the boundary under the action of the oncoming stream $V(U_\infty, V_\infty)$ where u_∞ is given by

$$u_\infty = K_0 V_\infty \tag{2.1}$$

with

$$K_0 = \tan\left(\frac{\pi}{2}\frac{L}{D}\right). \tag{2.2}$$

Here L is the length of each slat and D is the distance between the leading-edges of the two adjacent slats.

By letting L and D tend to zero simultaneously while keeping the ratio between them constant, he deduces the condition at the boundary as

$$\pm u = K_0 v \tag{2.3}$$

where the plus sign refers to the region above the wall while the minus sign to that below the wall. Note that the uniform velocity components V_∞ and u_∞ have been replaced by the local value v and u at the boundary by virtue of the limiting process.

It is a usual assumption that the static pressure in the plenum behind a perforated wall is equal to the freestream static pressure inside the tunnel. To incorporate this condition into his formulation, Brescia superimposes an open-jet boundary upon the cascade-

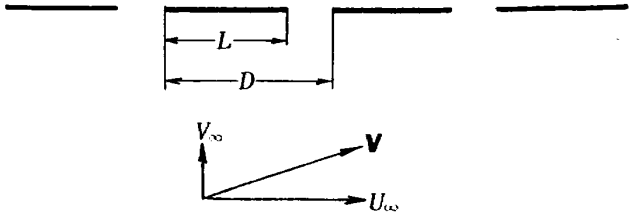

Sketch 1

like boundary and finds that the influence of the perforated wall on the flow field around a body represented by a combination of vortex and source singularities of strength, say, $A=Q+i\Gamma$ is expressed by an image singularity of strength $r\bar{A}$ where $\bar{A}$ is the complex conjugate of A and r is given as

$$r=\frac{2K_0+i}{2K_0-i}. \tag{2.4}$$

A mean boundary condition identical to (2.3) with (2.2) was also obtained by Maeder (refs. 21 & 22) assuming a uniform streamwise velocity increment along the slots and enforcing the Kutta's condition at the trailing-edge of each slat. Restricting the consideration to the interior of the wind tunnel, we thus have the equation

$$u+Kv=0 \tag{2.5}$$

as the mean boundary condition along the perforated wall. In the derivation of Brescia or Maeder, the value of the coefficient K is determined solely as a function of the open-to-total area ratio σ of the wall:

$$\sigma=1-L/D. \tag{2.6}$$

In fact, the usual practice in theoretical treatments of the perforated-wall-interference effects is to accept (2.5) but leave the value of K intact so that it is determined by some experimental procedure to give a certain amount of compensation for the over-simplifying nature of the mean boundary condition. This is seen from the following reasoning of (2.5): the effect of a perforated wall (i.e. an infinite series of transverse slots) at some distance from the wall is likened to that due to a series of aerofoils of infinitesimal chord-length placed at the location of the wall. The pressure difference across the aerofoils is proportional to the angle of attack $\alpha=v/(U_\infty+u)\sim v/U_\infty$:

$$\Delta C_p=\frac{p-p_c}{\frac{1}{2}\rho U_\infty{}^2}=2K\frac{v}{U_\infty} \tag{2.7}$$

where $2K$ is the constant of proportionality, and p_c is the static pressure in the plenum chamber. On the other hand, the pressure p is related to the streamwise velocity increment u via

$$\frac{p-p_\infty}{\frac{1}{2}\rho U_\infty{}^2}=-2\frac{u}{U_\infty}. \tag{2.8}$$

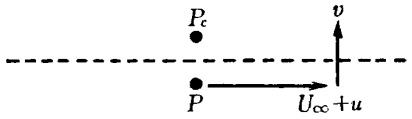

Sketch 2

Now assume that the plenum pressure p_c is equal to the free-stream static pressure p_∞:

$$p_c=p_\infty. \tag{2.9}$$

Then from equations (2.7) and (2.8) we obtain the mean boundary condition (2.5).

The value of K in (2.7) cannot be determined within the scope of the reasoning given above. Then the condition (2.7) can be interpreted as merely stating the assertion that the vertical velocity component v at the wall is proportional to the pressure difference across it. Since the constant of proportionality depends in reality on the structure of (and the boundary layer characteristics along) the wall, the value of K is best determined by some experimental measures on the particular wind tunnel one is concerned so as to describe the interference characteristics appropriately.

For the later reference we remark that the boundary condition (2.5) is satisfied by considering a suitable image of the body against the boundary just as is the case with a closed or open-jet boundary. This fact is already pointed out, e.g., in ref. 4, page 93 and is understood by the following reasoning: the condition (2.5) indicates that the perturbation velocity component in the direction of ($\cos A$, $\sin A$) vanishes identically along the wall where

$$A=\arctan(K). \tag{2.10}$$

Let us assume that the body inside the tunnel is represented by a singularity such as a source, a doublet or a vortex. Consider the image of the singularity with respect to the closed boundary. The perturbation velocity v_c due to this image induced at a point P on the boundary is symmetric, with respect to the boundary, to the velocity v_0 due to the original singularity. From simple geometrical considerations (sketch 3) it is seen that through the rotation by an angle of $2A-\pi$ in the counter-clockwise sense, the velocity vector v_c is brought to a position v in which it becomes symmetric to v_0 with respect to the line through P normal to the direction ($\cos A$, $\sin A$). Then v represents the effect of the perforated boundary, for v_0+v has no component in the direction ($\cos A$, $\sin A$). Since the angle of rotation $2A-\pi$ does not depend on the choice of a particular point P, the boundary condition along the perforated wall is thus satisfied by an image singularity derived from that for the closed wall through the rotation of angle $2A-\pi$.

In complex variables a rotation by an angle

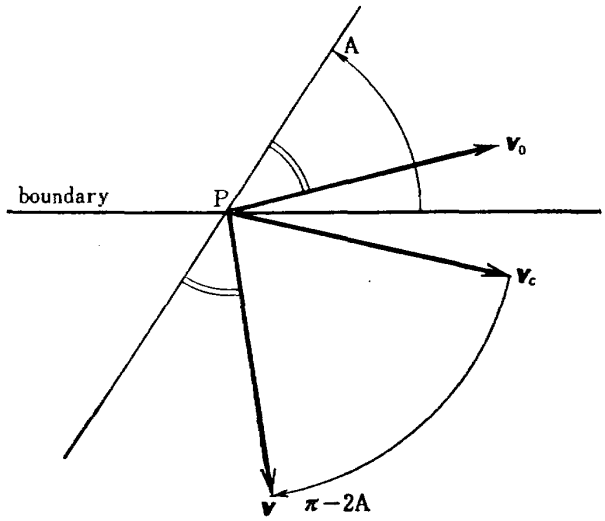

Sketch 3

of θ implies the multiplication by the factor $e^{i\theta}$. Hence the complex potential w due to the image in a perforated wall is obtained from the complex potential w_c due to the image in the closed wall by multiplying the latter with the factor $e^{i\delta}$:

$$w=e^{i\delta}\cdot w_c \qquad (2.11)$$

where

$$\delta=\pi-2A. \qquad (2.12)$$

Note that a rotation in a velocity vector is equivalent to the rotation in the corresponding complex potential of the same amount but of the opposite sense since the complex velocity is u-iv.

From (2.10) and (2.12) we have

$$e^{i\delta}=\frac{K+i}{K-i}. \qquad (2.13)$$

On the other hand, we have seen in eq. (2.4) and in the paragraph preceding it that Brescia obtained the factor r taking exactly the same line of thought. The coefficient K_0 in the factor r, which corresponds to our $e^{i\delta}$, is, however, accompanied by a factor of 2 unlike that in our expression (2.13). The source of this discrepancy has not been identified in view of the fact that the theoretical value of K is irrelevant to the actual calculation of the interference effects because what is used in the calculation is the relation (2.11), the value of δ (or r) to be determined by some experimental procedures.

2. 2. Experimental facts about perforated wall characteristics

Turning back to the mean boundary condition (2.5), we now examine its validity in the light of experimental facts. Experimental investigations of the boundary condition along perforated walls have been conducted by several people including Stokes et al. (ref. 23), Maeder (refs. 21 & 22) and Chen & Mears (ref. 24).

The experiment reported in ref. 23 was made using 2 inch-square piece of 0.35 inch-thick Plexiglas as the perforated material placed along one of the test-section walls of a 3 inch-square supersonic wind tunnel. The hole diameters ranged from 0.018 inch to 0.039 inch with corresponding open ratio from 14.8% to 36.5%. The results showed that a logarithmic plot of the pressure drop Δp across the material against the normal velocity v_n through it indicated a slope of 1.3 at a free-stream Mach number of 1.3. It might be argued that this relationship is fairly close to the linear one, $\Delta p \propto v_n$, and thus lends support to the validity of the boundary condition (2.5). It should be noted, however, that the experimental set-up, as can be seen from the above description, is rather remote from the actual conditions encountered on the test-section walls of conventional perforated wind tunnels. For one thing, the hole diameters are too small to be the representative of the actual condition, which is of order of 0.5 inch. For another, in view of the difference in the development of the boundary layer along the boundary between a solid wall and a perforated one (e.g. refs. 20 & 25), the state of the boundary layer on the 2 inch-square material may be quite different from what is found along the actual wind tunnel walls, which, as will be seen in the subsequent paragraphs, may lead to a conspicuous difference in the wall characteristics.

In refs. 21 & 22, results are given of measurements for a single transverse slot of 1 inch width and for a variety of perforated sheets of 4 inch $\times$ 5 inch size fitted into the test-section wall of a 4 inch $\times$ 8 inch low speed wind tunnel. Fig. 1 shows the measured results for the single transverse slot while Fig. 2 for the perforated sheets, both being taken from refs. 21 & 22. Fig. 1 illustrates that the mean boundary condition (2.5) describes fairly well the actual situation for single transverse slot. For a perforated boundary, the curves in Fig. 2 show essentially linear relationships between ΔC_p and v_n/U_∞, but there are appreciable displacements of curves to the right of the origin, which are the larger for the smaller values of the open ratio σ. Maeder argues (refs. 20,

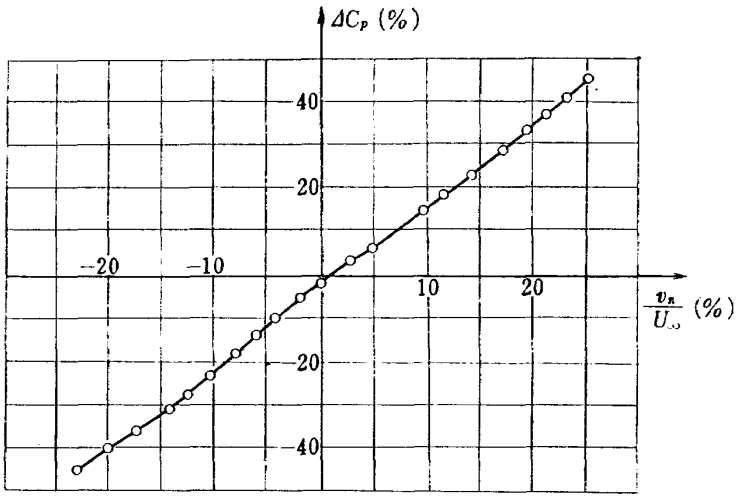

Fig. 1 Characteristics of a 1-inch Transverse Slot (reproduced from refs. 21 & 22)

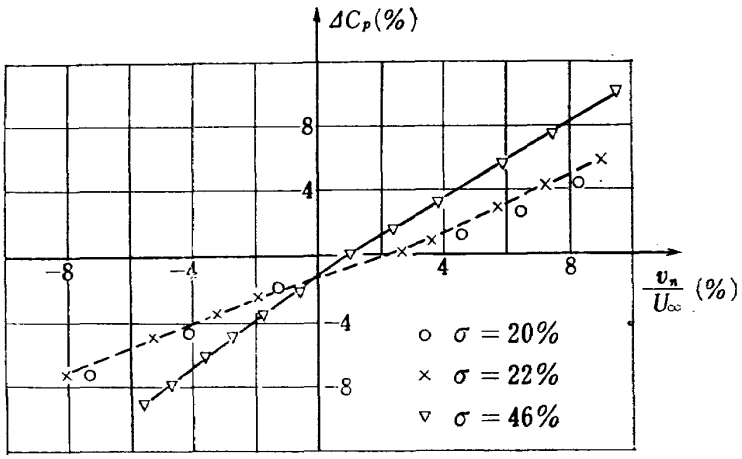

Fig. 2 Characteristics of Perforated Sheets (reproduced from refs. 21 & 22)

21 & 22) that this shift is due to the turbulent mixing along the perforated boundary. This explanation sounds plausible but is difficult to explain the larger displacements for the smaller open ratios. Presumably other mechanisms are also operating, but it is probable that the turbulent mixing is the major cause of this shift. In the two experiments referred to above, the measurements were taken at the tunnel-empty condition. Chen & Mears, on the other hand, measured perforated-wall characteristics with an aerofoil installed in the test section (ref. 24).

In their experiment, the roof of the solid-wall test section of a 22 inch × 32 inch low speed wind tunnel was removed and a perforated sheet of 22.5% open ratio (0.25 inch hole diameter) was fitted into the place. The effective height of the test section was then

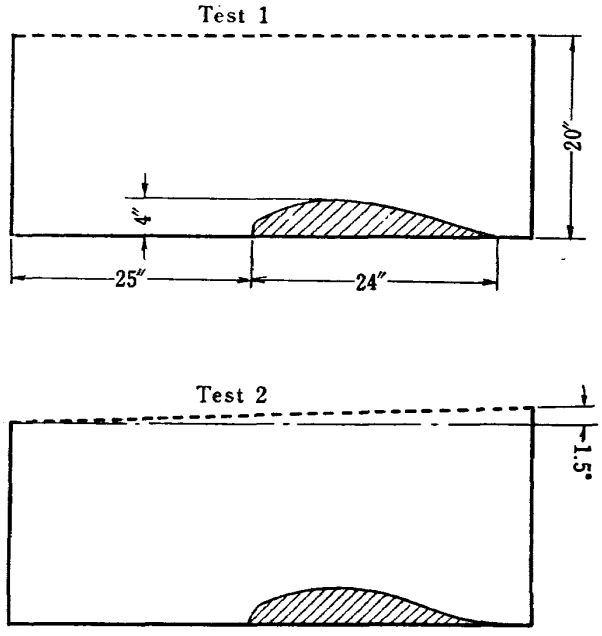

Sketch 4

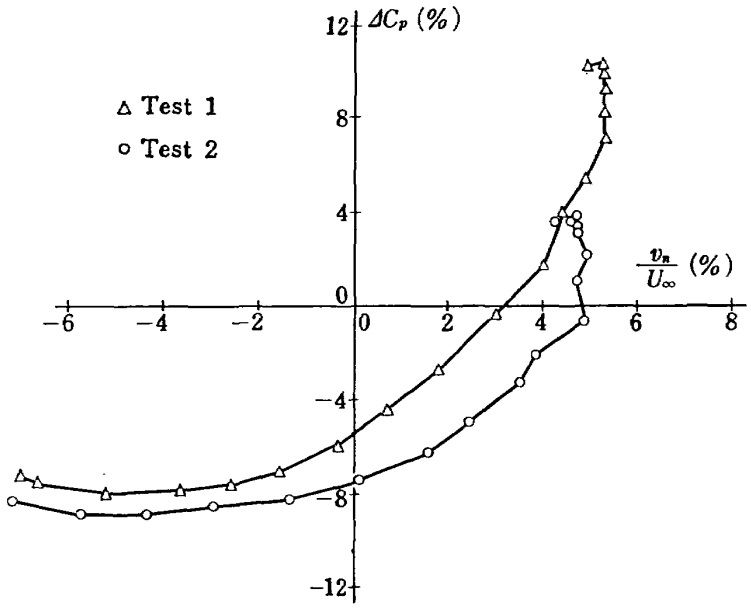

Fig. 3 Characteristics of Perforated Sheets under the Influence of an Aerofoil Model
(reproduced from ref. 24)

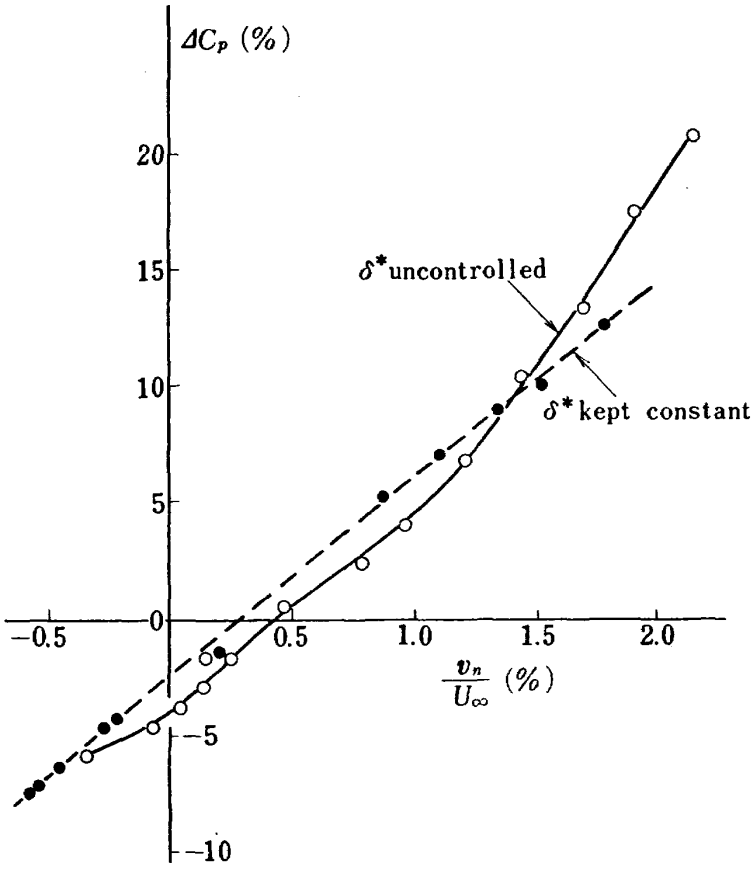

Fig. 4 Comparison of Perforated Wall Characteristics Determined under Constant and Variable Boundary Layer Thicknesses
(reproduced from ref. 26)

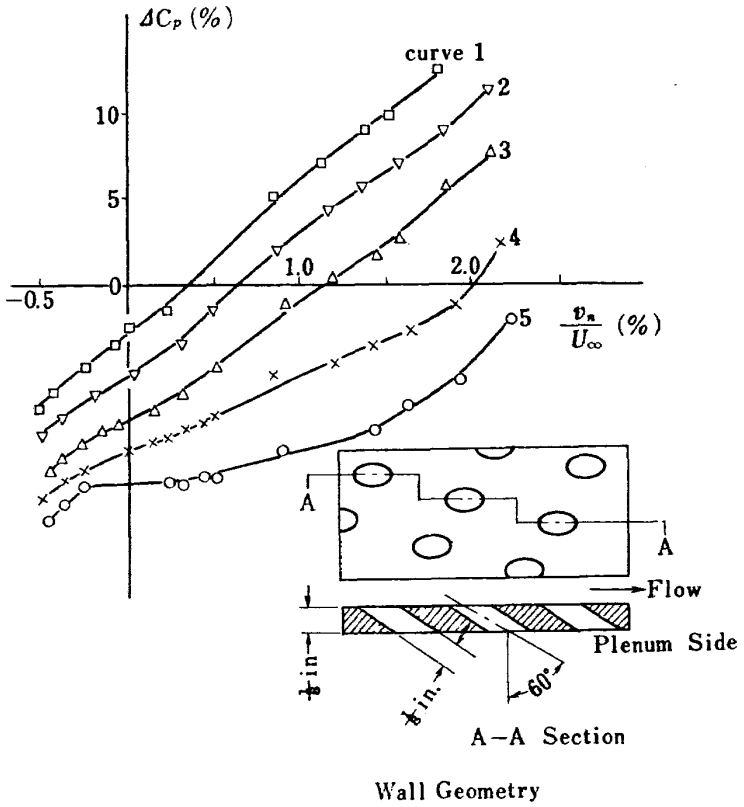

Fig. 5 Perforated Wall Characteristics for Various Boundary Layer Thicknesses (reproduced from ref. 26)

20 inch. A half Joukowsky aerofoil of 24 inch-chord and 4 inch-thickness was placed on the lower solid wall as shown in Sketch 4.

Part of the measured results is given in Fig. 3.

The marked nonlinearity of the $\Delta C_p \sim v_n/U_\infty$ curves in Fig. 3 makes a sharp contrast with the results obtained by Maeder (cf. Fig. 2).

The reason for this difference has not been identified partly because detailed experimental conditions such as the geometrical structure of the perforated sheets are not given for the experiment reported in ref. 21. At least, however, two factors are conceivable as the possible sources of discrepancy. The first is that the disturbances created by the aerofoil in Chen & Mear's experiment may have been too large compared with those encountered in the usual wind tunnel experiments since the aerofoil-thickness-to-tunnel-height ratio amounted to 0.2. The second is that the geometrical structure of the perforated wall relative to the thickness of the boundary layer along it is thought to have been quite different in both cases. That the effects of boundary layers on the perforated-wall characteristics are serious is seen, e.g., from the review given by Lukasiewicz (ref. 26). Figs. 4 & 5 are quoted from ref. 26, which were constructed by Lukasiewicz taking data from the work due to Chew. (W. L. Chew: AEDC-TN-55-44)

The usual experimental procedure of obtaining $\Delta C_p \sim v_n/U_\infty$ relation was to change values of ΔC_p and v_n/U_∞ by altering the wall inclination and the plenum chamber suction pressure while maintaining a constant flow speed within the test section. Fig. 4 indicates that caution must be exercised in interpreting the data obtained under such circumstances. The boundary layer thickness is not controlled in such procedure and the results may be such as the curve shown by the solid line in Fig. 4. Each experimental point defining the curve may correspond to different boundary layer thicknesses. If, on the other hand, the boundary layer thickness is controlled in obtaining $\Delta C_p \sim v_n/U_\infty$ curve, the relation may be such as shown by the broken line in Fig. 4. In Fig. 5 the curves 1 to 5 correspond to different boundary layer thicknesses, on each of the curves the displacement thickness δ^* of the boundary layer being kept constant. The value of δ^* for each curve is given below together with the ratio of δ^* to the hole diameter d.

Fig. 5 shows that the nonlinearity in the relation between ΔC_p and v_n/U_∞ increases as

curve No.	δ^*(in.)	δ^*/d
1	0.0535	0.428
2	0.0680	0.544
3	0.0827	0.662
4	0.1245	0.995
5	0.2990	2.39

the hole diameter d becomes smaller relative to the boundary layer thickness. Although these data are in fact obtained with 60°-inclined holes as is shown in the sketch inset in Fig. 5, qualitatively similar results are expected from the experiments for normal holes.

2. 3. Determination of the mean bounbary condition

One may conclude from the experimental facts outlined in the preceding sub-section the following:

(1) as far as Fig. 1 indicates, the mean boundary condition for a transverse slot is represented fairly well by eq. (2.5).

(2) In view of the results shown in Figs. 2, 3 and 5, the perforated-wall characteristics may not be represented by those of a series of transverse slots even in the two-dimensional situation.

(3) Perforated-wall characteristics depend critically on the geometrical structure of the wall, such as the wall thickness, the hole diameter and the hole spacing, in relation to the state of the boundary layer along the wall. If, for instance, the hole diameter is too small compared with the boundary layer thickness, the characteristics will exhibit marked nonlinearity.

(4) Even when the characteristics are essentially linear, the actual perforated-wall condition is different from eq. (2.5) in that the $\Delta C_p \sim v_n/U_\infty$ curve passes through $\Delta C_p=0$ at a positive value of v_n (i.e. there is a flow from the inside of the test section into the plenum chamber when the pressure difference is zero), a fact which, according to Maeder, is attributed to the turbulent mixing along a partly open boundary.

Thus it is desirable that the mean boundary condition for a perforated wall incorporates the possible nonlinearity in $\Delta C_p \sim v_n/U_\infty$ curve and the 'turbulent mixing' effect. Of the two, the nonlinearity makes the theoretical treatment of the interference analysis almost impossible whereas the inclusion of the 'turbulent mixing' effect may be relatively feasible since the resulting problem can be dealt with still within the scope of the linearized wall-interference theory. If, however, the ranges of the variation of ΔC_p and v_n/U_∞ are small, it is expected that the relation between them is represented fairly well by eq. (2.5) by adjusting the value of K appropriately. The validity of this conjecture may be proved or disproved by determining the value of K from particular experimental data and by seeing then whether this value of K also produces consistent results for other experimental data. In doing so, errors arising from other sources in predicting the characteristics of the flow field inside a wind tunnel must be kept sufficiently small so that the main portion of the discrepancy between the prediction and the experiment, if any, may be attributed to the defect in the construction of the theoretical model for the calculation of the wall-interference effects.

In the following section a theoretical procedure is established for the wall-interference calculation using the mean boundary condition given by eq. (2.5), which is supposed to be of sufficient accuracy in deciphering the interference effects upon the pressure distribution on an aerofoil.

III. FORMULAE FOR THE CALCULATION OF TWO-DIMENSIONAL WALL-INTERFERENCE EFFECTS IN A PERFORATED WIND TUNNEL

3. 1. Preliminaries

Let us fix the coordinate system within the test section of a wind tunnel so that the x-axis is aligned with the centre-line of the tunnel directed downstream and the y-axis is taken upward. Let H denote the test-section height. The interference problem within a perforated wind tunnel is then formulated using the disturbance potential φ as

$$\nabla^2\varphi=0 \tag{3.1}$$

with the boundary conditions

$$\frac{\partial\varphi}{\partial x}+K\frac{\partial\varphi}{\partial y}=0 \quad \text{at} \quad y=\frac{H}{2} \tag{3.2a}$$

and

$$\frac{\partial\varphi}{\partial x}-K\frac{\partial\varphi}{\partial y}=0 \quad \text{at} \quad y=-\frac{H}{2} \tag{3.2b}$$

which are the reiteration of (2.5). Note that for the lower wall, the normal velocity directed towards the outside of the tunnel is given by $-\partial\varphi/\partial y$.

The interference potential φ_1 is defined as the difference between φ and φ_0 where φ_0 is the disturbance potential at the free-air condition. Since φ_0 satisfies the Laplace equation, the formulation in terms of φ_1 is as follows:

$$\nabla^2\varphi_1=0, \tag{3.3}$$

$$\frac{\partial\varphi_1}{\partial x}+K\frac{\partial\varphi_1}{\partial y}=-\left(\frac{\partial\varphi_0}{\partial x}+K\frac{\partial\varphi_0}{\partial y}\right)$$

$$\text{at}\quad y=\frac{H}{2}\ ,\quad \text{and} \tag{3.4a}$$

$$\frac{\partial\varphi_1}{\partial x}-K\frac{\partial\varphi_1}{\partial y}=-\left(\frac{\partial\varphi_0}{\partial x}-K\frac{\partial\varphi_0}{\partial y}\right)$$

$$\text{at}\quad y=-\frac{H}{2}. \tag{3.4b}$$

To facilitate the use of the convenient relation (2.11), we introduce a complex variable notation $z=x+iy$. Consider a complex potential w_0 due to a singularity such as a source or a vortex in the free-air located at a point $z=z_0=x_0+iy_0$ given as

$$\frac{dw_0}{dz}=\frac{a}{z-z_0} \tag{3.5}$$

where a is a real constant when the singularity is a source while it is imaginary when the singularity is a vortex.

According to the relation (2.11), the image potential w_{0U} of w_0 with respect to the upper wall of the test section is given by

$$\frac{dw_{0U}}{dz}=e^{i\delta}\frac{\bar{a}}{z-[x_0+i(H-y_0)]} \tag{3.6}$$

whereas the image of w_0 with respect to the lower wall is

$$\frac{dw_{0L}}{dz}=e^{-i\delta}\frac{\bar{a}}{z-[x_0-i(H+y_0)]} \tag{3.7}$$

where the minus sign preceding $i\delta$ in (3.7) is due to the fact that the normal to the lower wall is directed downward (cf. eq. (3.2b)), and the bar over a indicates the complex conjugate. Considering the successive images of w_{0U}, w_{0L}, and so on, we obtain a sequence of image potentials from which the interference potential w_1 is derived as a series of them:

$$\begin{aligned}\frac{dw_1}{dz}=&\frac{\bar{a}e^{i\delta}}{z-[x_0+i(H-y_0)]}+\frac{\bar{a}e^{-i\delta}}{z-[x_0-i(H+y_0)]}\\&+\frac{(\overline{\bar{a}e^{-i\delta}})e^{i\delta}}{z-[x_0+i(2H+y_0)]}+\frac{(\overline{\bar{a}e^{i\delta}})e^{-i\delta}}{z-[x_0-i(2H-y_0)]}\\&+\frac{\overline{[(\bar{a}e^{i\delta})e^{-i\delta}]}e^{i\delta}}{z-[x_0+i(3H-y_0)]}+\frac{\overline{[(\bar{a}e^{-i\delta})e^{i\delta}]}e^{-i\delta}}{z-[x_0-i(3H+y_0)]}\\&+\cdots\cdots\end{aligned}$$

$$\begin{aligned}=&\bar{a}\sum_{n=1}^{\infty}\left[\frac{e^{(2n-1)i\delta}}{z-\bar{z}_0-(2n-1)iH}+\frac{e^{-(2n-1)i\delta}}{z-\bar{z}_0+(2n-1)iH}\right]\\&+a\sum_{n=1}^{\infty}\left[\frac{e^{2ni\delta}}{z-z_0-2niH}+\frac{e^{-2ni\delta}}{z-z_0+2niH}\right].\end{aligned} \tag{3.8}$$

Suppose that φ_0 on the right-hand side of (3.4) is given as the real part of w_0 defined by (3.5). Then the solution φ_1 of (3.3) with the boundary condition (3.4) is identical with the real part of w_1 given by (3.8).

It is convenient to determine the range of variation of the parameter δ before proceeding to the evaluation of w_1. From equation (2.10) it is seen that the angle A assumes the following values for the closed and the open-jet boundaries:

$$A=\begin{cases}\pi/2 & \text{for the closed wall } (K\to\infty),\\ 0 & \text{for the open-jet boundary } (K=0).\end{cases} \tag{3.9}$$

Correspondingly the limiting values of δ for these cases are, from (2.12),

$$\delta=\begin{cases}0 & \text{for the closed wall,}\\ \pi & \text{for the open-jet boundary.}\end{cases} \tag{3.10}$$

The value of δ corresponding to a positive value of K falls within the interval $0<\delta<\pi$. Hence it is sufficient to consider the value of w_1 for the range $0\leq\delta\leq\pi$.

Now put

$$\begin{aligned}S_1=&\sum_{n=1}^{\infty}\left[\frac{e^{(2n-1)i\delta}}{z-\bar{z}_0-(2n-1)iH}+\frac{e^{-(2n-1)i\delta}}{z-z_0+(2n-1)iH}\right]\\=&2\sum_{n=1}^{\infty}\frac{(z-\bar{z}_0)\cos(2n-1)\delta-(2n-1)H\sin(2n-1)\delta}{(z-\bar{z}_0)^2+[(2n-1)H]^2}\end{aligned} \tag{3.11}$$

and

$$\begin{aligned}S_2=&\sum_{n=1}^{\infty}\left[\frac{e^{2ni\delta}}{z-z_0-2niH}+\frac{e^{-2ni\delta}}{z-z_0+2niH}\right]\\=&2\sum_{n=1}^{\infty}\frac{(z-z_0)\cos 2n\delta-2nH\sin 2n\delta}{(z-z_0)^2+(2nH)^2}.\end{aligned} \tag{3.12}$$

The series S_1 and S_2 can be expressed in terms of elementary functions by invoking either the Mittag-Leffler's theorem in the theory of functions or the analytic continuation of the Fourier series expansion of the function e^{cx} in the interval $(0, 2\pi)$.

Thus putting

$$\xi_1=\pi\frac{z-\bar{z}_0}{2H},\quad \xi_2=\pi\frac{z-z_0}{2H} \tag{3.13}$$

and

$$\kappa=\delta/\pi, \tag{3.14}$$

we obtain the following expressions for S_1

and S_2:
for $0<\delta<\pi$:

$$S_1(z, z_0) = -\frac{\pi}{2H}\frac{e^{(2z-1)\xi_1}}{\cosh(\xi_1)}, \quad (3.15\text{a})$$

$$S_2(z, z_0) = \frac{\pi}{2H}\left\{\frac{e^{(2z-1)\xi_2}}{\sinh(\xi_2)} - \frac{1}{\xi_2}\right\}; \quad (3.16\text{a})$$

for $\delta=0$:

$$S_1(z, z_0) = \frac{\pi}{2H}\tanh(\xi_1), \quad (3.15\text{b})$$

$$S_2(z, z_0) = \frac{\pi}{2H}\left\{\coth(\xi_2) - \frac{1}{\xi_2}\right\}; \quad (3.16\text{b})$$

and for $\delta=\pi$:

$$S_1(z, z_0) = -\frac{\pi}{2H}\tanh(\xi_1), \quad (3.15\text{c})$$

$$S_2(z, z_0) = \frac{\pi}{2H}\left\{\coth(\xi_2) - \frac{1}{\xi_2}\right\}. \quad (3.16\text{c})$$

Using S_1 and S_2, w_1 is written as

$$\frac{dw_1}{dz}(z, z_0) = \bar{a}S_1(z, z_0) + aS_2(z, z_0). \quad (3.17)$$

3. 2. Basic formulae

In a rigorous approach, the aerofoil could be represented by a distribution of vortices along its contour and the interference velocity would be obtained by a superposition of element interference velocities determined from the application of (3.17) to each of the element vortices. This approach, however, entails a considerable amount of computation, which does not seem warranted in view of the inference that the interference characteristics at a point near the model can be calculated with sufficient accuracy employing the linearized-theory approach. This inference is based on the following speculation.

The interference effects are identified with the change in the state of the flow field near the model which is caused by exacting a constraint due to the presence of the tunnel wall upon the flow at the position of the wall. To what extent would this change be affected by the error due to the replacement of the actual model with the system of singularities which is obtained from the linearized theory? Let c and t be respectively the chord-length and the maximum thickness of the aerofoil. At points where the constraint due to the tunnel wall is imposed on the flow, the ratio of the error referred to above in the disturbance velocities to the magnitude of the disturbance velocities themselves is at most of the order of $(c/H)^2(t/c)$, which is less than 1% in the usual test conditions. It is likely that the effects of the tunnel wall are felt at the model position to much lesser degree than at the position of the wall itself. Hence the relative error in the interference effects at the model position introduced by replacing the actual model with its linearized-theory representation is considered to be of a magnitude much smaller than the order of $(c/H)^2(t/c)$.

Therefore we may fall back on the thin-aerofoil theory and use the results obtained up to the relation (3.17) in order to derive both the blockage and the lift effects on an aerofoil mounted to the wind tunnel along the line $y=y_0$.

Let the origin of the coordinates be such that the leading-edge of the aerofoil is located on the y-axis. The free-air potential w_0 due to an aerofoil is given within the scope of the linearized theory as

$$w_0(z;\ y_0) = \frac{U_\infty}{\pi}\int_0^c [q(x_0) + i\gamma(x_0)]\log(z-z_0)dx_0 \quad (3.18)$$

where $q(x_0)$ ane $\gamma(x_0)$ are the strengths of source and vortex respectively, located at a point $x=x_0$. For the free-air condition they are given by

$$q=q_0(x_0)=\left(\frac{dy_t}{dx}\right)_{x=x_0} \quad (3.19)$$

and

$$\gamma=\gamma_0(x_0) = \sqrt{\frac{c-x_0}{x_0}}\left\{\alpha + \frac{1}{\pi}\int_0^c \sqrt{\frac{\xi}{c-\xi}} \times \frac{\left(\frac{dy_c}{dx}\right)_{x=\xi}}{x_0-\xi} d\xi\right\} \quad (3.20)$$

where α denotes the incidence, y_t the thickness distribution and y_c the camber of the aerofoil respectively.

The complex velocity $V_0=u_0-iv_0$ is then

$$V_0(z;\ y_0) = \frac{U_\infty}{\pi}\int_0^c [q(x_0) + i\gamma(x_0)]\frac{dx_0}{z-z_0}. \quad (3.21)$$

Comparing (3.21) with (3.5) and referring to (3.17), we see that the interference velocity $V_1=u_1-iv_1$ corresponding to the free-air velocity V_0 is given by

$$V_1(z; y_0) = \frac{U_\infty}{\pi}\left\{\int_0^c q(x_0)[S_1(z, z_0) + S_2(z, z_0)]dx_0 - i\int_0^c \gamma(x_0)[S_1(z, z_0) - S_2(z, z_0)]dx_0\right\}. \quad (3.22)$$

Except the case where $y=y_0=0$, the imaginary parts of both S_1+S_2 and S_1-S_2 are non-vanishing, which implies that the thickness part of the aerofoil gives rise to v_1 which ex-

presses the combined angle-of-attack- and streamline-curvature effects, while the incidence-camber part contributes to u_1 which indicates the blockage effect. In other words, coupling takes place between the thickness term and the lift effects, and between the incidence-camber term and the blockage effect. In the majority of the two-dimensional tests, however, the model is mounted to the wind tunnel along the centre-line of the test section, in which case we may put $y_0=0$ so that in calculating the interference effects at the aerofoil position ($y=y_0$), both S_1 and S_2 become real numbers thus leading to no coupling.

Restricting ourselves henceforth to the case where $y=y_0=0$, the velocities $V_0=u_0-iv_0$ and $V_1=u_1-iv_1$ at the aerofoil position are obtained from (3.21) and (3.22) respectively by taking the limits as $y\to 0$:

$$\frac{V_0(x,0)}{U_\infty}=\gamma(x)\,\mathrm{sign}\,(y)+\frac{1}{\pi}\oint_0^c\frac{q(x_0)}{x-x_0}\,dx_0 -i\left\{q(x)\,\mathrm{sign}\,(y)-\frac{1}{\pi}\oint_0^c\frac{\gamma(x_0)}{x-x_0}\,dx_0\right\} \tag{3.23}$$

provided x lies between 0 and c, and

$$\frac{V_1(x,0)}{U_\infty}=\frac{1}{H}\int_0^c q\,(x_0)\left[\frac{e^{2(\kappa-1)\xi_0}}{\sinh(2\xi_0)}-\frac{1}{2\xi_0}\right]dx_0 +\frac{i}{H}\int_0^c\gamma(x_0)\left[\frac{e^{2\kappa\xi_0}}{\sinh(2\xi_0)}-\frac{1}{2\xi_0}\right]dx_0 \tag{3.24}$$

where sign (y) is equal to $+1$ or to -1 according as the limit is taken keeping y positive or negative, and where κ is defined by (3.14) while $\oint$ denotes the Cauchy integral. ξ_0 is given by

$$\xi_0=\pi\frac{x-x_0}{2H}. \tag{3.25a}$$

Hence the disturbance velocity components u and v within the tunnel are written as

$$\frac{u}{U_\infty}=\frac{u_0+u_1}{U_\infty}=\gamma(x)\,\mathrm{sign}\,(y)+\frac{1}{\pi}\oint_0^c\frac{q(x_0)}{x-x_0}\,dx_0 +\frac{1}{H}\int_0^c q\,(x_0)\left[\frac{e^{2(\kappa-1)\xi_0}}{\sinh(2\xi_0)}-\frac{1}{2\xi_0}\right]dx_0$$

and

$$\frac{v}{U_\infty}=\frac{v_0+v_1}{U_\infty}=q(x)\,\mathrm{sign}\,(y)-\frac{1}{\pi}\oint_0^c\frac{\gamma(x_0)}{x-x_0}\,dx_0 -\frac{1}{H}\int_0^c\gamma(x_0)\left[\frac{e^{2\kappa\xi_0}}{\sinh(2\xi_0)}-\frac{1}{2\xi_0}\right]dx_0.$$

Let ξ, t and λ be defined as

$$\xi=\frac{x}{c},\quad t=\frac{x_0}{c}\quad\text{and}\quad\lambda=\frac{c}{H}. \tag{3.25b}$$

Rewriting in these variables u and v become

$$\frac{u}{U_\infty}=\gamma(\xi)\,\mathrm{sign}\,(y)+\frac{1}{\pi}\oint_0^1\frac{q(t)}{\xi-t}\,dt +\lambda\int_0^1 q(t)\left[\frac{e^{(\kappa-1)\tau}}{\sinh\tau}-\frac{1}{\tau}\right]dt \tag{3.26a}$$

and

$$\frac{v}{U_\infty}=q(\xi)\,\mathrm{sign}\,(y)-\frac{1}{\pi}\oint_0^1\frac{\gamma(t)}{\xi-t}\,dt -\lambda\int_0^1\gamma\,(t)\left[\frac{e^{\kappa\tau}}{\sinh\tau}-\frac{1}{\tau}\right]dt \tag{3.26b}$$

where $\tau=\pi\lambda(\xi-t)$.

Since the boundary condition along the aerofoil surface is

$$\frac{v}{U_\infty}=\frac{dy_t}{dx}\,\mathrm{sign}\,(y)-\alpha+\frac{dy_c}{dx}, \tag{3.27}$$

we obtain, by equating (3.26b) and (3.27),

$$q(\xi)=\left(\frac{dy_t}{dx}\right)_{x=c\xi} \tag{3.28}$$

and

$$-\frac{1}{\pi}\oint_0^1\frac{\gamma(t)}{\xi-t}\,dt-\lambda\int_0^1\gamma(t)\,K(\xi,t)\,dt=-\alpha+\frac{dy_c}{dx} \tag{3.29}$$

where

$$K(\xi,t)=\frac{e^{\kappa\cdot\kappa\lambda(\xi-t)}}{\sinh[\pi\lambda(\xi-t)]}-\frac{1}{\pi\lambda(\xi-t)} =\kappa+\lambda\frac{\pi}{6}(3\kappa^2-1)\,(\xi-t) +\lambda^2\frac{\pi^2}{6}\kappa(\kappa^2-1)\,(\xi-t)^2+\cdots\cdots \tag{3.30}$$

Equation (3.28) shows that the source strength $q(\xi)$ which represents the effect of the symmetrical part of the aerofoil is still given in terms of the slope of the aerofoil thickness just as is the case in the free-air condition. This is also true for an aerofoil mounted at any off-centre position. On the other hand, equation (3.29), which is an integral equation for the unknown $\gamma(t)$, indicates that the vortex strength $\gamma(t)$ is affected by the presence of the tunnel wall, the effect being manifested through the second integral on the left-hand side of (3.29).

In the usual situation, the aerofoil-chord-to-tunnel-height ratio λ is a small quantity, and we may expand $\gamma(t)$ in a power series of λ:

$$\gamma(t)=\gamma_0(t)+\gamma_1(t)\cdot\lambda+\gamma_2(t)\cdot\lambda^2+\cdots\cdots. \tag{3.31}$$

Substituting this expansion together with (3.30) into (3.29), we obtain the following

system of equations from which $\gamma_0, \gamma_1, \gamma_2, \cdots$ are determined successively.

$$-\frac{1}{\pi}\int_0^1 \frac{\gamma_0(t)}{\xi-t}\,dt=-\alpha+\frac{dy_c}{dx},$$

$$-\frac{1}{\pi}\int_0^1 \frac{\gamma_1(t)}{\xi-t}\,dt=\kappa\int_0^1 \gamma_0(t)\,dt,$$

$$-\frac{1}{\pi}\int_0^1 \frac{\gamma_2(t)}{\xi-t}\,dt=\kappa\int_0^1 \gamma_1(t)\,dt + \frac{\pi}{6}(3\kappa^2-1)\int_0^1 \gamma_0(t)\,(\xi-t)\,dt,$$

$$-\frac{1}{\pi}\int_0^1 \frac{\gamma_3(t)}{\xi-t}\,dt=\kappa\int_0^1 \gamma_2(t)\,dt + \frac{\pi}{6}(3\kappa^2-1)\int_0^1 \gamma_1(t)\,(\xi-t)\,dt + \frac{\pi^2}{6}\kappa(\kappa^2-1)\int_0^1 \gamma_0(t)\,(\xi-t)^2 dt$$

etc. (3.32)

To accommodate the Kutta's condition at the trailing edge, each of γ_n's must satisfy the following condition:

$$\gamma_n(1)=0 \quad \text{for all} \quad n=0,1,2,\cdots\cdots. \tag{3.33}$$

Since a solution of

$$\frac{1}{\pi}\int_0^1 \frac{f(t)}{\xi-t}\,dt=F(\xi)$$

for a function $F(\xi)$ continuous in (0,1) is given (e.g. ref. 27) by

$$f(t)=-\frac{1}{\pi}\sqrt{\frac{1-t}{t}}\int_0^1 \sqrt{\frac{s}{1-s}}\,\frac{F(s)}{t-s}\,ds+\frac{C}{\sqrt{t(1-t)}}$$

with an arbitrary constant C, the explicit forms of $\gamma_0, \gamma_1, \cdots$ are successively obtained from equations (3.32) with the condition (3.33). They are

$$\gamma_0(t)=\sqrt{\frac{1-t}{t}}\left\{\alpha+\frac{1}{\pi}\int_0^1 \sqrt{\frac{s}{1-s}}\,\frac{\left(\frac{dy_c}{dx}\right)_{x=cs}}{t-s}\,ds\right\}, \tag{3.34a}$$

$$\gamma_1(t)=\sqrt{\frac{1-t}{t}}\,\pi\kappa\left(c_1-\frac{\alpha}{2}\right), \tag{3.34b}$$

$$\gamma_2(t)=\sqrt{\frac{1-t}{t}}\,\pi^2\left\{\frac{9\kappa^2+1}{48}\alpha-\frac{3\kappa^2+1}{12}c_1 - \frac{3\kappa^2-1}{6}c_2-\frac{3\kappa^2-1}{6}\left(\frac{\alpha}{2}-c_1\right)t\right\}, \tag{3.34c}$$

$$\gamma_3(t)=\sqrt{\frac{1-t}{t}}\,\pi^3\kappa\left\{\frac{3\kappa^2+1}{48}c_1+\frac{\kappa^2+1}{12}c_2 + \frac{\kappa^2-1}{6}c_3-\frac{5\kappa^2+1}{96}\alpha-\left(\frac{\kappa^2}{6}c_1+\frac{\kappa^2-1}{3}c_2 - \frac{3\kappa^2-1}{24}\alpha\right)t-\frac{\kappa^2-1}{6}\left(c_1-\frac{\alpha}{2}\right)t^2\right\}, \tag{3.34d}$$

and so on, where

$$c_1=\frac{1}{\pi}\int_0^1 \sqrt{\frac{s}{1-s}}\left(\frac{dy_c}{dx}\right)_{x=cs} ds, \tag{3.35a}$$

$$c_2=\frac{1}{\pi}\int_0^1 \sqrt{\frac{s}{1-s}}\left(s-\frac{1}{2}\right)\left(\frac{dy_c}{dx}\right)_{x=cs} ds \tag{3.35b}$$

and

$$c_3=\frac{1}{\pi}\int_0^1 \sqrt{\frac{s}{1-s}}\left(s^2-\frac{1}{2}s-\frac{1}{8}\right)\left(\frac{dy_c}{dx}\right)_{x=cs} ds. \tag{3.35c}$$

Put

$$\lambda\int_0^1 \gamma(t)\,K(\xi,t)\,dt=g_0+g_1\frac{d}{d\xi}\xi(1-\xi) + g_2\frac{d}{d\xi}\xi^2(1-\xi)+\cdots\cdots \tag{3.37}$$

and define $\Delta\alpha$ and Δy_c by

$$\Delta\alpha=-g_0, \tag{3.38}$$

$$\frac{d}{dx}(\Delta y_c)_{x=c\xi}=g_1\frac{d}{d\xi}\xi(1-\xi) + g_2\frac{d}{d\xi}\xi^2(1-\xi)+\cdots\cdots. \tag{3.39}$$

Then (3.29) is expressed as

$$-\frac{1}{\pi}\int_0^1 \frac{\gamma(t)}{\xi-t}\,dt=-(\alpha+\Delta\alpha) + \left[\frac{d}{dx}(y_c+\Delta y_c)\right]_{x=c\xi}. \tag{3.40}$$

In (3.29), the case of $\lambda=c/H\to 0$ corresponds to the free-air condition. Comparing (3.40) and (3.29) with $\lambda=0$, we see that the aerofoil in the tunnel behaves as if it were placed in free-air with an incidence $\alpha+\Delta\alpha$ and the camber $y_c+\Delta y_c$. In other words, $\Delta\alpha$ and Δy_c denote the wall interference effects on the incidence and camber respectively. The coefficients g_0, g_1, $\cdots$, which give $\Delta\alpha$ and Δy_c are obtained by substituting (3.34) into the left-hand side of (3.37). Thus we have

$$\Delta\alpha=\kappa\left(c_1-\frac{\alpha}{2}\right)(\pi\lambda)+\left(\frac{9\kappa^2+1}{48}\alpha-\frac{3\kappa^2+1}{12}c_1 - \frac{3\kappa^2-1}{6}c_2\right)(\pi\lambda)^2+\kappa\left(\frac{2\kappa^2+1}{36}c_1 + \frac{\kappa^2+1}{12}c_2+\frac{\kappa^2-1}{6}c_3-\frac{7\kappa^2+2}{144}\alpha\right) \times(\pi\lambda)^3+O(\lambda^4) \tag{3.41}$$

and

$$\frac{\Delta y_c}{c}=\left\{\frac{3\kappa^2-1}{12}\left(c_1-\frac{\alpha}{2}\right)(\pi\lambda)^2+\kappa\left(\frac{4\kappa^2-1}{72}\alpha - \frac{5\kappa^2+1}{72}c_1-\frac{\kappa^2-1}{6}c^2\right)(\pi\lambda)^3\right\}\xi(1-\xi) + \frac{\kappa(\kappa^2-1)}{18}\left(c_1-\frac{\alpha}{2}\right)(\pi\lambda)^3\xi^2(1-\xi)+O(\lambda^4) \tag{3.42}$$

where the symbol $O(\lambda^4)$ indicates terms at

most of the order of λ^4.

So far the solution of equation (3.29) has been treated and the lift effects $\Delta\alpha$ and Δy_c are obtained as above. We now turn to the evaluation of the blockage effect which manifests itself through the streamwise interference velocity u_1.

Within the frame work of the present formulation, the 'wake blockage' cannot be obtained since the presence of the wake is not taken into account at all. In the usual situation of tests for streamlined bodies, however, this effect is extremely small and we may safely neglect it compared with other interference effects.

The solid blockage, on the other hand, is readily calculated from the expression (3.24) for V_1. Denoting the solid blockage factor (the ratio of u_1 to the free-stream velocity U_∞) by ε_s, and employing the notation defined in (3.25b), we have

$$\varepsilon_s=\lambda\int_0^1 q(t)\left[\frac{e^{(\kappa-1)\tau}}{\sinh(\tau)}-\frac{1}{\tau}\right]dt. \tag{3.43}$$

Expanding the function in the square bracket in (3.43) into a power series of λ, we obtain

$$\varepsilon_s=\lambda\left\{\left[\frac{1}{4}\left(\kappa^2-2\kappa+\frac{2}{3}\right)(\pi\lambda)+\frac{\kappa}{6}(\kappa-1)(\kappa-2)(\pi\lambda)^2\cdot\xi\right]\frac{S_W}{c^2}-\frac{\kappa}{6}(\kappa-1)(\kappa-2)(\pi\lambda)^2\frac{M_W}{c^3}\right\}+O(\lambda^4) \tag{3.44}$$

where S_W is the aerofoil sectional area:

$$S_W=2\int_0^c y_t dx \tag{3.45a}$$

and M_W is the aerofoil-thickness moment of area about the leading-edge:

$$M_W=2\int_0^c x\cdot y_t dx. \tag{3.45b}$$

Equation (3.44) shows that up to the third power of λ, ε_s varies linearly with x in the streamwise direction. We can devide ε_s into the average blockage factor $\bar{\varepsilon}_s$ over the aerofoil chord and the term $c(d\varepsilon_s/dx)$ which represents the buoyant effect due to the streamwise pressure gradient:

$$\bar{\varepsilon}_s=\frac{1}{4\pi}\left(\kappa^2-2\kappa+\frac{2}{3}\right)\frac{S_W}{c^2}(\pi\lambda)^2+\frac{\kappa}{12\pi}(\kappa-1)(\kappa-2)\left(\frac{S_W}{c^2}-2\frac{M_W}{c^3}\right)(\pi\lambda)^3+O(\lambda^4) \tag{3.46}$$

and

$$c\frac{d\varepsilon_s}{dx}=\frac{\kappa}{6\pi}(\kappa-1)(\kappa-2)\frac{S_W}{c^2}(\pi\lambda)^3+O(\lambda^4). \tag{3.47}$$

These formulae agree with the results of ref. 5 except the term proportional to M_W, which has been neglected in ref. 5 because there the aerofoil was replaced by a concentrated singularity.

Equations (3.46) and (3.47) together with (3.41) and (3.42) give a complete description of the interference effects within the range of the present formulation.

3. 3. Comparison with the concentrated-singularity approach

In the usual procedure of the conventional wall-interference theories, the aerofoil thickness is replaced by a doublet situated at the centroid of the aerofoil in obtaining the solid blockage effect whilst the effects on the incidence and camber are computed using a concentrated vortex located at the centre of pressure on the aerofoil.

The expressions of the interference velocities due to these concentrated singularities are readily obtained by putting

$$q(x_0)=\pi r_0^2\delta'(x_0-x_c) \tag{3.48a}$$

and

$$\gamma(x_0)=(\Gamma/2U_\infty)\delta(x_0-x_p) \tag{3.48b}$$

into (3.24), where r_0 denotes the radius of the circle represented by the doublet, x_c and x_p the x-coordinates of the centroid and the centre of pressure respectively, Γ the circulation around the aerofoil, $\delta(x)$ the Dirac's delta and $\delta'(x)$ being its derivative.

Denoting by $\bar{u}_1$ and $\bar{v}_1$ the interference velocity components thus calculated, we have

$$\bar{u}_1(x)=-U_\infty r_0^2\left\{\frac{\partial}{\partial x_0}[S_1(x,x_0)+S_2(x,x_0)]\right\}_{x_0=x_c}=U_\infty\pi^2\left(\frac{r_0}{H}\right)^2\left\{\frac{1}{\xi_c^2}+\kappa\frac{e^{(\kappa-1)\xi_c}}{\sinh(\xi_c)}-\frac{e^{\kappa\xi_c}}{\sinh^2(\xi_c)}\right\} \tag{3.49a}$$

and

$$\bar{v}_1(x)=\frac{\Gamma}{2\pi}[S_1(x,x_0)-S_2(x,x_0)]_{x_0=x_p}=\frac{\Gamma}{2H}\left[\frac{1}{\xi_p}-\frac{e^{\kappa\xi_p}}{\sinh(\xi_p)}\right] \tag{3.49b}$$

where

$$\xi_c=\pi\frac{x-x_c}{H}\quad\text{and}\quad\xi_p=\pi\frac{x-x_p}{H}. \tag{3.50}$$

The expressions (3.49 a, b) are valid for both $\kappa=0$ (closed-wall) and $\kappa=1$ (open-jet boundary). Note that for the latter case, a uni-

form normal velocity component $\Gamma/(2H)$ has been superimposed on $\bar{v}_1$ to offset the non-vanishing $\lim_{x\to-\infty}\bar{v}_1$ so that the uniform flow far upstream becomes parallel to the tunnel axis.

Congruent with the approximation in which the aerofoil thickness is represented by a doublet while the incidence and camber by a vortex, it is a practice to calculate the solid blockage $\bar{u}_1$, the buoyancy effect $d\bar{u}_1/dx$, the incidence change $\bar{v}_1$ and the streamline curvature effect $d\bar{v}_1/dx$, all at the mid-chord position $x=x_m$.

Tus we have, to the first order of $(x_m-x_c)/H$ and $(x_m-x_p)/H$, the following:

$$\varepsilon_s=\left(\frac{\bar{u}_1}{U_\infty}\right)_{x=x_m}=\pi^2\left(\frac{r_0}{H}\right)^2\left\{\frac{1}{2}\left(\kappa^2-2\kappa+\frac{2}{3}\right)+\frac{\pi}{6}\kappa(\kappa-1)(\kappa-2)\frac{x_m-x_c}{H}\right\}, \quad (3.51\,a)$$

$$\frac{c}{U_\infty}\left(\frac{d\bar{u}_1}{dx}\right)_{x=x_m}=\pi^2\left(\frac{c}{H}\right)\left(\frac{r_0}{H}\right)^2\left\{\frac{\pi}{3}\kappa(\kappa-1)(\kappa-2)+\pi^2\left(\frac{\kappa^4}{4}-\kappa^3+\kappa^2+\frac{2}{15}\right)\frac{x_m-x_c}{H}\right\}, \quad (3.51\,b)$$

$$\Delta\alpha=\left(\frac{\bar{v}_1}{U_\infty}\right)_{x=x_m}=-\frac{\Gamma}{2HU_\infty}\left\{\kappa+\frac{\pi}{6}(3\kappa^2-1)\frac{x_m-x_c}{H}\right\} \quad (3.52\,a)$$

and

$$\frac{\Delta y_c/c}{\xi(1-\xi)}=\frac{c}{2U_\infty}\left(\frac{d\bar{v}_1}{dx}\right)_{x=x_m}=-\frac{\pi\Gamma}{4U_\infty c}\left(\frac{c}{H}\right)^2\left\{\frac{3\kappa^2-1}{6}+\pi\frac{\kappa(\kappa^2-1)}{3}\frac{x_m-x_p}{H}\right\}. \quad (3.52\,b)$$

Comparing (3.51 a, b) with (3.46) and (3.47), we see that r_0 and x_m correspond to S_W and M_W as

$$r_0^2\sim\frac{S_W}{2\pi} \quad \text{and} \quad \frac{x_m-x_c}{c}\sim 1-2\frac{M_W}{S_W c}. \quad (3.53)$$

On the other hand, since

$$\Gamma=2U_\infty\int_0^c\gamma(x)dx=2\pi U_\infty c\left\{\left(\frac{\alpha}{2}-c_1\right)-\frac{\kappa}{2}\left(\frac{\alpha}{2}-c_1\right)(\pi\lambda)+\left(\frac{3\kappa^2+1}{48}\alpha-\frac{\kappa^2+1}{16}c_1-\frac{3\kappa^2-1}{12}c_2\right)\times(\pi\lambda)^2+\cdots\cdots\right\}, \quad (3.54)$$

comparison of (3.52 a) and (3.41) shows that the two expressions agree with each other up to the order of $(\pi\lambda)^2$ if the following relation holds:

$$\frac{x_m-x_p}{c}=\frac{\int_0^1\left(\frac{1}{2}-t\right)\gamma_0(t)dt}{\int_0^1\gamma_0(t)dt} \quad (3.55\,a)$$

whereas the comparison (3.52 b) and (3.42) indicates that

$$\frac{x_m-x_p}{c}=\frac{\int_0^1\left(\frac{1}{3}-t\right)\gamma_0(t)dt}{\int_0^1\gamma_0(t)dt} \quad (3.55\,b)$$

if both be to coincide up to the order of $(\pi\lambda)^3$.

Using the relations

$$\Gamma=\frac{1}{2}U_\infty c C_L$$

and

$$x_m-x_p=\frac{1}{4}c\left(1+4\frac{C_m}{C_L}\right), \quad (3.56)$$

(3.52) can be rewritten as

$$\frac{\Delta\alpha}{C_L}=-\lambda\left[\frac{\kappa}{4}+\pi\frac{3\kappa^2-1}{96}\left(1+4\frac{Cm}{C_L}\right)\lambda\right] \quad (3.57)$$

and

$$\frac{1}{C_L}\frac{\Delta y_c/c}{\xi(1-\xi)}=-\lambda\left[\frac{3\kappa^2-1}{48}(\pi\lambda)+\frac{\kappa(\kappa^2-1)}{96}\left(1+4\frac{C_m}{C_L}\right)(\pi\lambda)^2\right] \quad (3.58)$$

where C_L is the lift coefficient and C_m is the moment coefficient about the quarter-chord point.

This concentrated-singularity approach requires the values of r_0, Γ and x_p to be given from other considerations. For the latter two, it is usual to connect them with the *measured* values of C_L and C_m via the relations (3.56). For the former, on the other hand, there are many alternative expressions so far proposed corresponding to various cross-sectional shapes of the tunnel test section. (e.g., see ref. 28) With the thin-aerofoil approach taken in the present paper, on the contrary, no data are needed in computing the wall-interference characteristics except for the aerofoil geometry and the value of the factor κ.

The difference in the calculated results between the two approaches can be identified by collating the formulae (3.46), (3.47), (3.41) and (3.42) with (3.51a, b), (3.57) and (3.58). Although the difference has been obscured by the introduction of C_L and C_m to replace Γ

and x_p, the less accurate nature of the concentrated-singularity approach is illustrated through the conditions (3.55 a) and (3.55 b). We observe that if the relations (3.56) are to be used with the measured values of C_L and C_m then the centre of pressure x_p should be given by

$$\frac{x_p}{c}=\int_0^1 t\gamma(t)\,dt \Big/ \int_0^1 \gamma(t)\,dt$$

i.e. by using $\gamma(t)$ and not by using $\gamma_0(t)$ as has been done in (3.55 a). Also, the discrepancy between (3.55 a) and (3.55 b) reveals the fact that the accuracy of the formula (3.52 b), and hence possibly of (3.58), is not guaranteed beyond the leading term in either expression.

IV. APPLICATION TO THE NAL 2m×2m TRANSONIC WIND TUNNEL

4. 1. Experimental set-up

The purpose of the present investigation is to find the value of the porosity parameter P, which is defined as

$$P=1/K \qquad (4.1)$$

and which is related to the factor κ via

$$P=\tan\left(\frac{\pi}{2}\kappa\right), \qquad (4.2)$$

for the transonic test section of our 2m×2m wind tunnel and see whether this value is consistently applied to the calculation of the interference characteristics.

For this purpose, data are assembled for the pressure distributions on aerofoils measured within the Tunnel at various Mach numbers and incidences.

The prototype test section of the Tunnel is of the type whose four walls are perforated at about 20% open-area ratio with 12mm-diameter normal holes through the 12-mm-thick wall plate.*

Two aerofoil models of NACA 65_2-215 and NACA 64A214 sections both of 350mm chord-length were installed to this test section spanning the full breadth of 2m. A kind of masking tape was applied to the inside of the side walls to seal them thus rendering them effectively closed walls.

Later, this test section was furnished with four aluminium plates, each of which was superimposed on each of the four walls, with the objective of making the test section a variable-open-area-ratio one. These plates have the same perforation geometry as the test-section walls and can be slid relative to the walls so that the effective open-area ratio is varied continuously from 20% to 0.

A third model of 10.5% thickness ratio and 400 mm chord-length, named Model 70811, was tested in this version of the test section by setting the side-wall-open-area-ratio to zero. Fig. 6 shows the test section installed with this model. Ref. 29 is to be referred to for a detailed description of the Tunnel, and ref. 30 for a description of the aerofoil section used for the Model 70811.

The gaps between the model ends and the side walls were carefully sealed using rubber gaskets to prevent the upper surface flow from communicating with the lower surface one. As a check of the two-dimensionality of the flow, the chordwise pressure distribution at the quarter-span station was measured on the Model 70811 and was compared with that at the mid-span station. Fig. 7 shows one of the results of the comparison where the solid lines indicate the mid-span distribution while the small circular symbols represent the quarter-span distribution.

As is seen from the Figure, the two-dimensionality is thought to be good for this test.

4. 2. Method of analysis

The analysis given in Section III has been carried out under the assumption of the incompressible flow. Obviously the interference effects depend on the Mach number and so does the porosity parameter $P=1/K$.

The effects of compressibility in the interference calculation can be taken into account via the Prandtl-Glauert transformation, which is considered to be a good approximation in view of the argument given at the beginning of 3. 2.

The wall-interference problem in a compressible flow is written as

$$\begin{cases} \beta^2\dfrac{\partial^2\varphi}{\partial x^2}+\dfrac{\partial^2\varphi}{\partial y^2}=0 \quad (\beta=\sqrt{1-M_\infty^2}), & (4.3) \\ \dfrac{\partial\varphi}{\partial x}\pm K\dfrac{\partial\varphi}{\partial y}=-\left(\dfrac{\partial\varphi_0}{\partial x}\pm K\dfrac{\partial\varphi_0}{\partial y}\right) \\ \qquad\qquad \text{at} \quad y=\pm\dfrac{H}{2}. & (4.4) \end{cases}$$

* Later, a variable-open-area-ratio test section has become available which enables us to set the open-area ratio at an arbitrary value between 0 and 8% independently for each of the two horizontal walls as well as for the vertical walls.

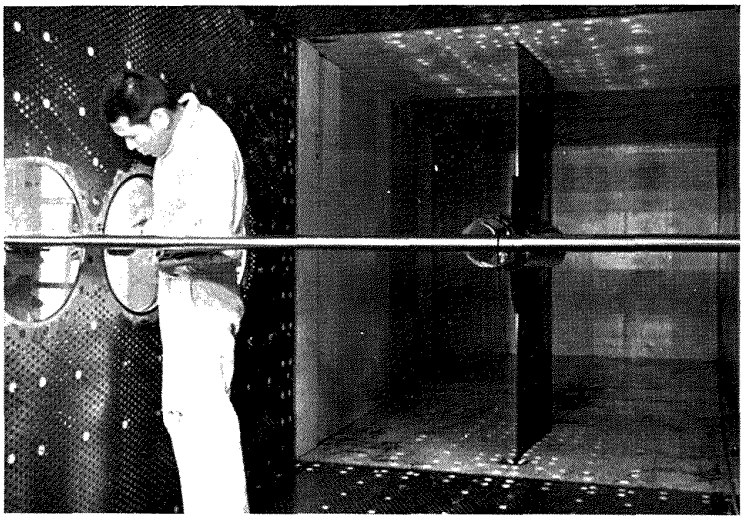

Fig. 6 The test section of the NAL 2 m×2 m wind tunnel with the Model 70811 installed

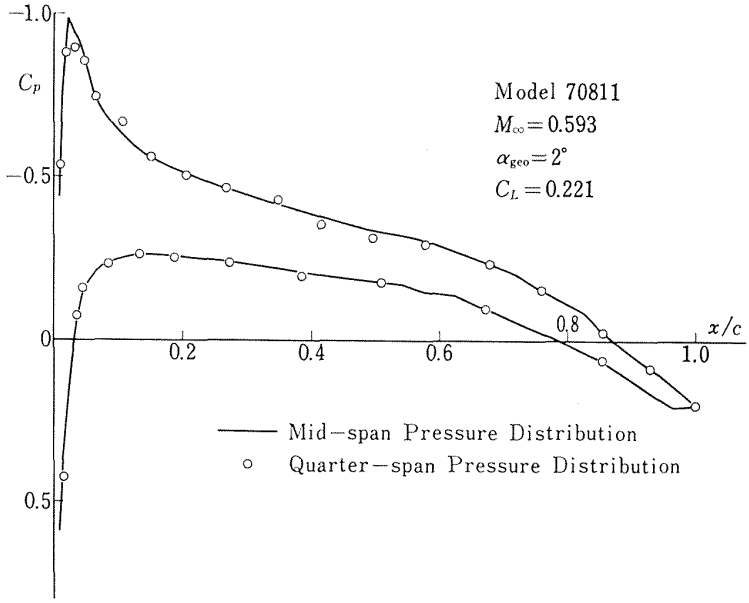

Fig. 7 Two-dimensionality of the Test Data

According to the transformation, the solution $\varphi(x, y; K, H)$ of the above equation for a given aerofoil is related to the interference potenal $\varphi_i(\xi, \eta; K_i, H_i)$ in incompressible flow for the same aerofoil via

$$\varphi(x, y; K, H)=\frac{1}{\beta}\varphi_i(\xi, \eta; \beta K, \beta H)\Big|_{\substack{\xi=x \\ \eta=\beta y}}. \tag{4.5}$$

Consequently, the velocity components are written as

$$u(x, y)=\frac{1}{\beta}u_i(x, \beta y; \beta K, \beta H) \tag{4.6}$$

and

$$v(x, y)=v_i(x, \beta y; \beta K, \beta H) \tag{4.7}$$

where the subscript i denotes the quantity in incompressible flow.

Putting

$$\cot\left(\frac{\pi}{2}\kappa_i\right)=\beta K \tag{4.8}$$

and observing from (4.5) that $c/H=\lambda$ should be replaced by $c/(\beta H)=\lambda/\beta$, we therefore obtain from (3.41), (3.42), (3.46) and (3.47) the following formulae for the wall-interference effects in compressible flow:

$$\begin{aligned}\Delta\alpha=&\frac{\kappa_i}{\beta}\left(c_1-\frac{\alpha}{2}\right)(\pi\lambda)+\frac{1}{\beta^2}\left(\frac{9\kappa_i^2+1}{48}\alpha-\frac{3\kappa_i^2+1}{12}c_1\right.\\&\left.-\frac{3\kappa_i^2-1}{6}c_2\right)(\pi\lambda)^2+\frac{\kappa_i}{\beta^3}\left(\frac{2\kappa_i^2+1}{36}c_1+\frac{\kappa_i^2+1}{12}c_2\right.\\&\left.+\frac{\kappa_i^2-1}{6}c_3-\frac{7\kappa_i^2+2}{144}\alpha\right)(\pi\lambda)^3\\&+\frac{1}{\beta^4}O(\lambda^4),\end{aligned} \tag{4.9}$$

$$\frac{\Delta y_c}{c}=\left\{\frac{3\kappa_i^2-1}{12}\frac{1}{\beta^2}\left(c_1-\frac{\alpha}{2}\right)(\pi\lambda)^2\right.$$

$$+\frac{1}{\beta^3}\kappa_i\left(\frac{4\kappa_i^2-1}{72}\alpha-\frac{5\kappa_i^2+1}{72}c_1-\frac{\kappa_i^2-1}{6}c_2\right)(\pi\lambda)^3\Big\}\xi(1-\xi)+\frac{1}{\beta^3}\frac{\kappa_i(\kappa_i^2-1)}{18}\left(c_1-\frac{\alpha}{2}\right)(\pi\lambda)^3\xi^2(1-\xi)+\frac{1}{\beta^4}O(\lambda^4), \tag{4.10}$$

$$\bar{\varepsilon}_s=\frac{1}{\beta^3}\frac{1}{4\pi}\left(\kappa_i^2-2\kappa_i+\frac{2}{3}\right)\frac{S_W}{c^2}(\pi\lambda)^2+\frac{1}{\beta^4}\frac{\kappa_i(\kappa_i-1)(\kappa_i-2)}{12\pi}\left(\frac{S_W}{c^2}-2\frac{M_W}{c^3}\right)(\pi\lambda)^3+\frac{1}{\beta^5}O(\lambda^4) \tag{4.11}$$

and

$$c\frac{d\varepsilon_s}{dx}=\frac{1}{\beta^4}\frac{\kappa_i(\kappa_i-1)(\kappa_i-2)}{6\pi}\frac{S_W}{c^2}(\pi\lambda)^3+\frac{1}{\beta^5}O(\lambda^4). \tag{4.12}$$

Suppose that the value of the porosity parameter $P=1/K$ is known for a Mach number M_∞. Then the value of the factor κ_i is determined from eq. (4.8), and the interference characteristics for the Mach number M_∞ are calculated using eqs. (4.9) through (4.12). Conversely, if the interference effects are known for a Mach number, then the value of the porosity parameter for that Mach number can be obtained by retracing the above procedure.

Now the interference effects are found by comparing the measured values with the 'true' values of lift, moment, pressure, and so on. Thus the problem of finding the value of the porosity parameter is reduced to that of finding the true values of these quantities in relation to the associated measured values.

For the purpose of finding the true value in the pressure distribution on an aerofoil, a theoretical procedure has been developed based on the works reported in refs. 1 and 2.

This procedure predicts the flow velocity V along the aerofoil surface via the formula

$$\frac{V}{U_\infty}=\frac{1+[(V/U_\infty)_i\sqrt{1+\theta^2}-1]/B_W}{\sqrt{1+(\theta/B_W)^2}} \tag{4.13}$$

where θ denotes the aerofoil slope, $(V/U_\infty)_i$ the velocity (ratio) on the same aerofoil submerged in incompressible flow which can be calculated to the desired accuracy by, e.g., the Theodorsen-Garrick procedure, and where B_W is the Wilby factor given by

$$B_W=\sqrt{1-M_\infty^2(1-M_\infty C_{pi})}$$

using the pressure coefficient C_{pi} in incompressible flow:

$$C_{pi}=1-(V/U_\infty)_i^2.$$

The effects of viscosity, on the other hand, are taken into account through the 'boundary-layer camber model', i.e., by modifying the aerofoil incidence and camber conforming to the displacement effects of the boundary layers on the aerofoil surface.

A detailed description of this procedure is given in ref. 32, hence no further accounts will be given here. But it is noted that, as has been demonstrated in ref. 32, the procedure, provided the flow on the aerofoil is subcritical and attached, enables one to calculate the pressure distribution on an aerofoil with an accuracy of less than about 2% error in the value of the lift coefficient in the usual situations, and of at most about 5% error in a most critical condition. Since the wall-interference effects amount to around 20% or more in the values of lift for the usual situation of tests made in the 20% open-area-ratio test section of our 2m×2m wind tunnel, the procedure is thought to be accurate enough to impart reasonable accuracy to the value of the porosity parameter determined by taking the pressure distribution calculated by it as the 'true' value.

The value of the porosity parameter, therefore, is determined in the following manner for each of the experimental pressure distribution data: the theoretical pressure distributions are calculated for an appropriately chosen range of κ_i taking into account the wall-interference effects by correcting the free-stream Mach number against the blockage effect using (4.11) and modifying the aerofoil incidence and camber according to (4.9) and (4.10). Then the measured value of the lift coefficient is compared with the theoretical ones thus calculated. Finally the value of κ_i (and hence of the porosity parameter P) is fixed to the one for which the theoretical lift agrees with the measured one.

4.3. Results of analysis

We note that in the procedure outlined in the preceding sub-section, only the lift data are explicitly used in finding the value of κ_i. Hence the validity of the present wall-interference calculation scheme is judged, on one hand, from the value of κ_i determined in the manner described above and on the other, by comparing the experimental pressure distribution with the theoretical one, the value

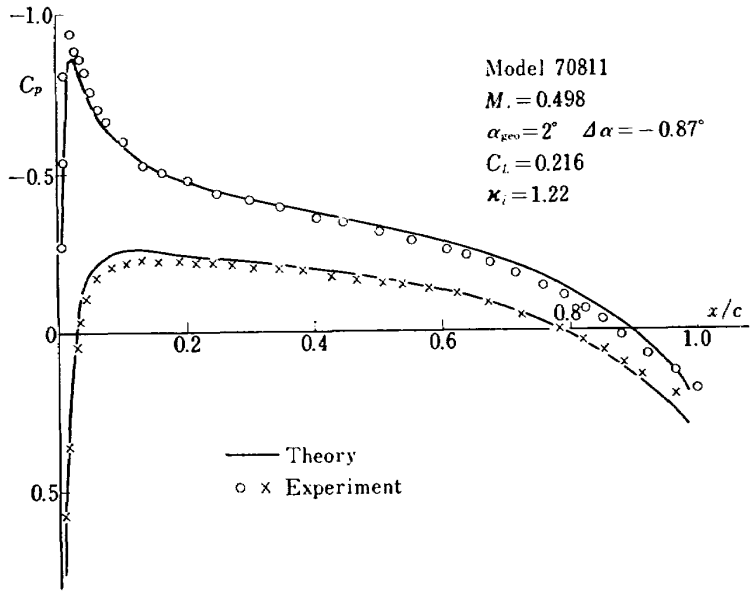

Fig. 8 (a) Pressure Distributions on Model 70811, $M_\infty=0.5$, $\alpha=2°$

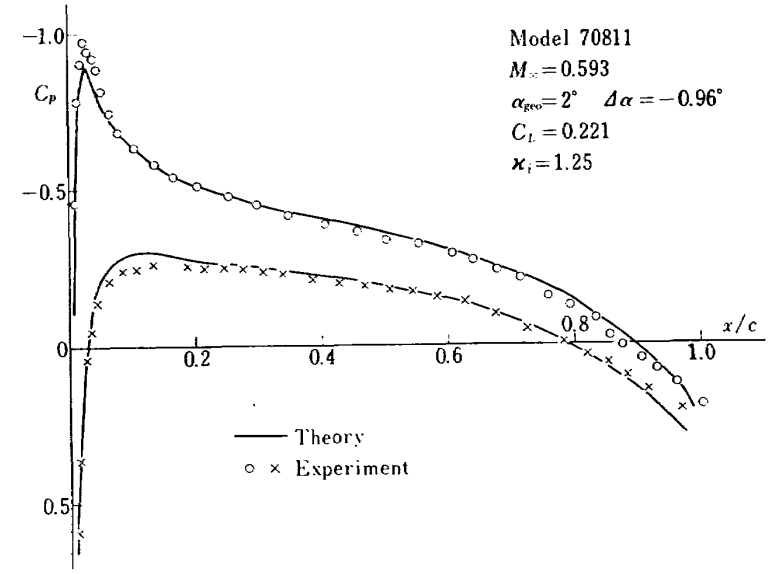

Fig. 8 (b) Pressure Distributions on Model 70811, $M_\infty=0.6$, $\alpha=2°$

of the lift coefficients in both cases coinciding with each other.

The figures to follow illustrate part of this comparison. Figs. 8 (a) to (c) show the results for the Model 70811 at an incidence of 2° for three different free-stream Mach numbers. To obtain the theoretical lift coefficients which are the same as the experimental ones, the values of κ_i had to be taken as 1.22, 1.25 and 1.22 for Mach numbers 0.5, 0.6 and 0.7 respectively. The corresponding values of the interference effect in the incidence, which is by far the largest among the four interference effects,* are given in each of the figures as $\Delta\alpha$.

Now from the stand-point of the wall-interference characteristics, a perforated test section is thought to behave as an intermediate between the closed wall and the open-jet boundary. Then κ_i should satisfy the inequality $0\leq\kappa_i\leq1$ in view of its definition (4.8) since the porosity parameter $P=1/K$ is zero for the closed wall and is infinitely large for the open-jet boundary, in between being always positive. A value of κ_i greater than unity corresponds to a negative value of P (or K).

* The following data may be of use to illustrate the order of magnitude of each of the interference effects, which correspond to the case shown in Fig. 8(b):

(1) $\Delta\alpha=-0.96°$ against the given geometrical incidence $\alpha_{geo}=2°$ thus reducing the effective incidence to the sheer 1.04°.

(2) $\Delta y_c/c=-0.0023\xi(1-\xi)-0.0005\xi^2(1-\xi)$.

(3) $\bar{\varepsilon}_s=-0.0012$.

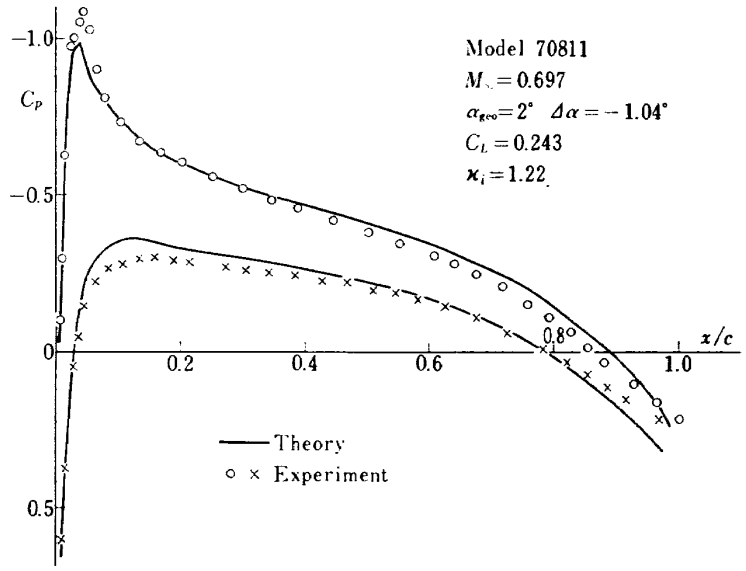

Fig. 8 (c) Pressure Distributions on Model 70811, $M_\infty = 0.7$, $\alpha = 2°$

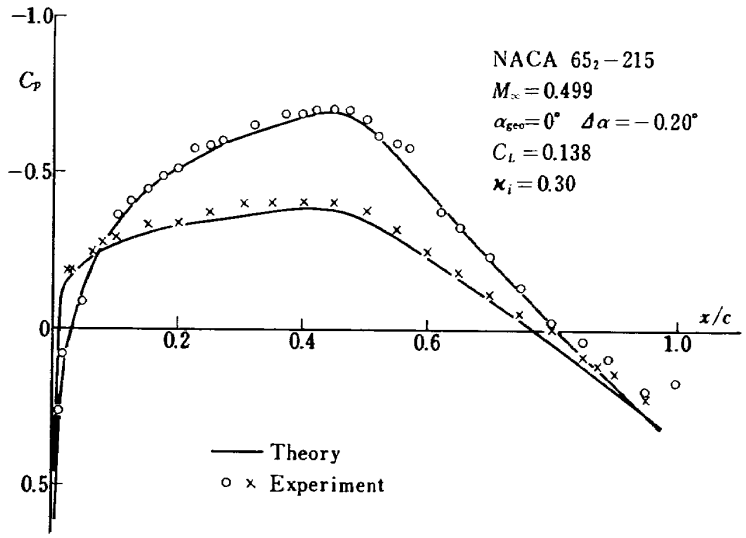

Fig. 9 (a) Pressure Distributions on the NACA 65_2-215 Model, $M_\infty = 0.5$, $\alpha = 0°$

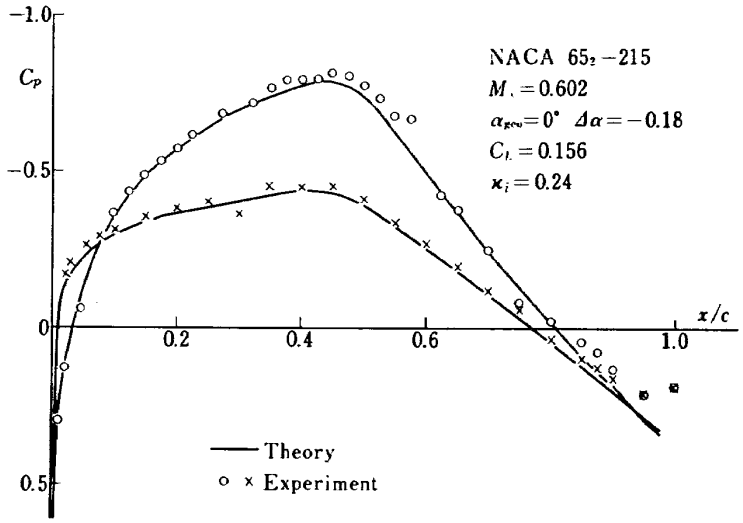

Fig. 9 (b) Pressure Distributions on the NACA 65_2-215 Model, $M_\infty = 0.6$, $\alpha = 0°$

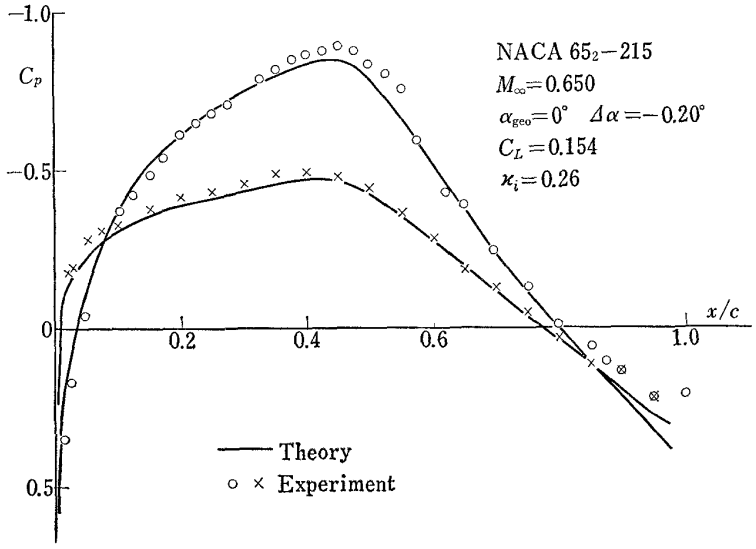

Fig. 9 (c) Pressure Distributions on the NACA 65_2–215 Model, $M_\infty=0.65, \alpha=0°$

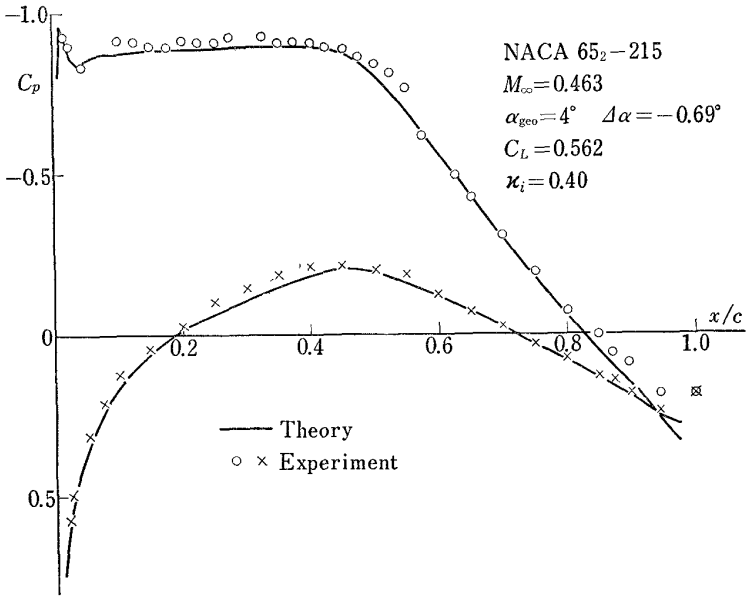

Fig. 9 (d) Pressure Distributions on the NACA 65_2–215 Model, $M_\infty=0.46$, $\alpha=4°$

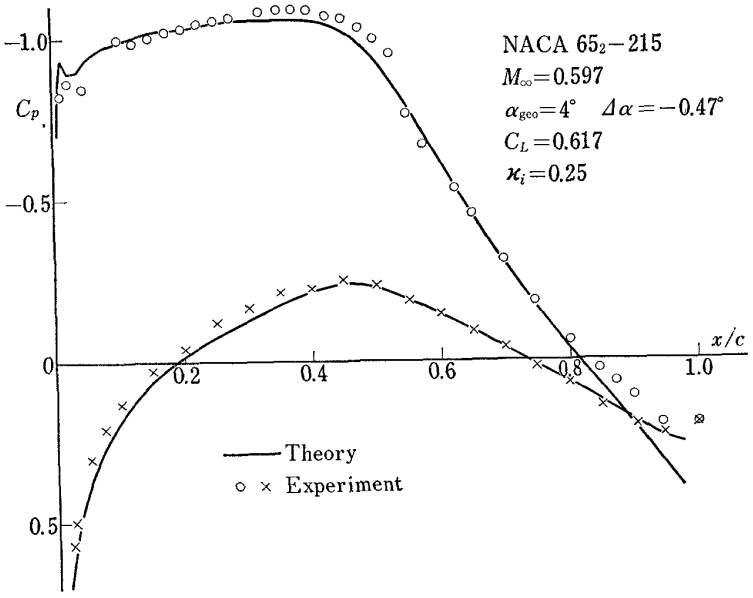

Fig. 9 (e) Pressure Distributions on the NACA 65_2–215 Model, $M_\infty=0.6, \alpha=4°$

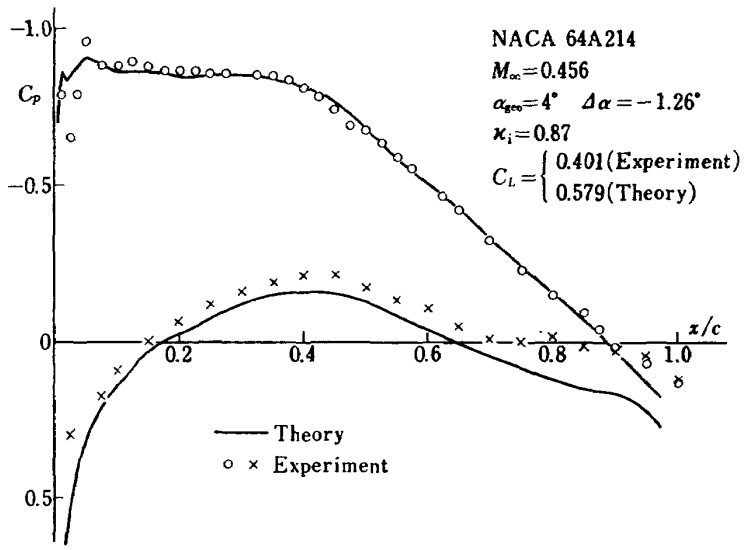

Fig. 10 (a) Pressure Distributions on the NACA 64A214 Model, M_∞=0.46,α=4°

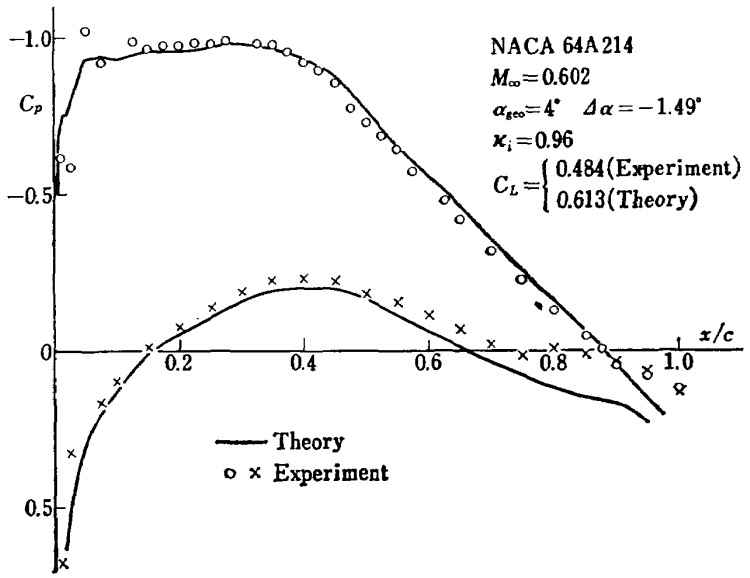

Fig. 10 (b) Pressure Distributions on the NACA 64A214 Model, M_∞=0.6,α=4°

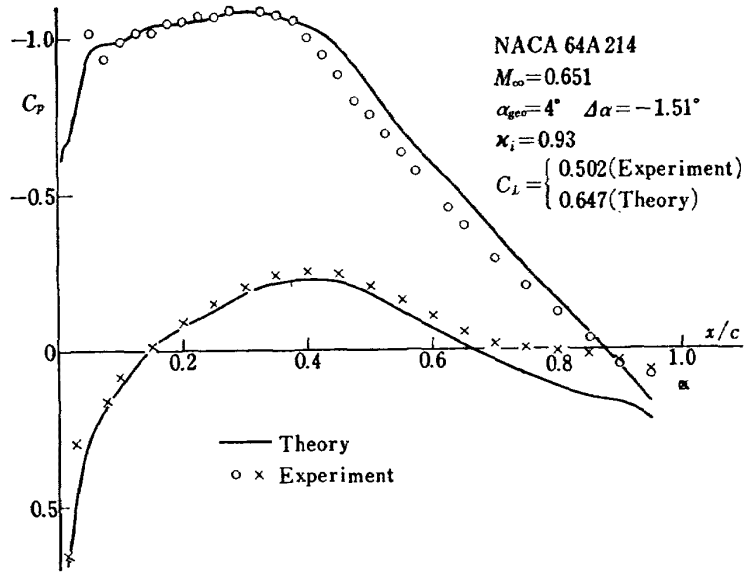

Fig. 10 (c) Pressure Distributions on the NACA 64A214 Model, M_∞=0.65, α=4°

Referring to the boundary condition (3.2), a negative value of K implies a flow through the boundary in the direction inverse to the pressure gradient across it. Recognizing the accuracy of the theoretical method of obtaining the pressure distribution and hence the lift coefficient, one is led from this observation to doubt the validity of the boundary condition (3.2), or equivalently (4.4), for the perforated test section.

Before discussing the matter further, let us have a look at the results for the other two aerofoil models. Figs. 9 (a) to (e) show the case of the NACA 65_2–215 model. Of these, (a) to (c) are concerned with the case of 0° incidence while (d) and (e) are of 4° incidence.

As is seen from the values of κ_i given in each of these figures, there is a wide scatter among them, which are essentially to be dependent only on the free-stream Mach number. (In the present situation the Reynolds number and the state of the boundary layers along the tunnel walls are almost uniquely determined by the Mach number.)

In fact the theoretical data shown in Fig. 9 are somewhat less reliable than those in Fig. 8 because, as is seen from the experimental pressure distributions, separation of flow, though in a small scale, has taken place in the cases of Fig. 9 (a) to (c) near the trailing edge of the model, and because with the cases of (d) and (e) the flow is on the verge of a large-scale separation on the rear part of the upper surface. In both of these circumstances part of accuracy may be lost in the theoretical method. However, the inconsistency in the values of κ_i is far greater than what can be attributed to the uncertainty in the theoretical prediction.

For the case of the NACA 64A214 model shown in Figs. 10 (a) to (c), the intention to match the theoretical and experimental lift coefficients was abandoned in view of the irregularity in the experimental pressure distributions on the rear part of the lower surface. Instead, an attempt has been made to bring the theoretical pressure distributions on the upper surface to coincide with the experimental ones as close as possible by adjusting the value of κ_i.

If it were attempted to match the values of the lift, much greater values of κ_i than those given in Fig. 10 would have resulted since the theoretical lift values are still almost 30% larger than the experimental values even after the correction of the incidence corresponding to those values of κ_i given in the figures.

4. 4. Discussion

Before launching the actual calculation of κ_i, it was expected that the values of κ_i obtained from the data on the three different aerofoil models for the same Mach number would coincide with each other since the porosity parameter P, and hence κ_i, was thought to depend only on the free-stream Mach number. It was further anticipated from the definition (4.8) that the variation of κ_i with the free-stream Mach number M_∞ would resemble the curve given by

$$\sqrt{1-M_\infty^2}\tan[(\pi/2)\kappa_i]=\text{const}$$

because the porosity parameter would not vary appreciably with the free-stream Mach number as long as the latter was kept within a reasonably small range well below unity. As a matter of fact, the calculated results have come against these anticipations as was already seen in the preceding sub-section.

Then, what is to blame for this contradiction? To identify the source of the contradiction, we first list the chief ingredients of the present wall-interference analysis as follows:

(1) The basic model for the interference calculation, i.e., equations (4.3) and (4.4).
(2) The method of solution for the interference model, i.e., the thin-aerofoil approach described in the sub-section 3.2.
(3) The experiments.
(4) The theoretical calculation of the pressure distribution on an aerofoil in compressible viscous flow, i.e, the method given in ref. 32.

Of these, neither (2) nor (4) are likely to be so inaccurate that they would cause the glaring inconsistency in the values of κ_i which is actually experienced.

For the experiments, a degree of uncertainty is admitted about the data on the NACA 65_2–215 model, which were obtained under somewhat incomplete conditions. That is, the sealing of the side walls may not have been complete due to peeling off of part of the tape caused by a strong pressure difference across the walls. The ineffectiveness in sealing, however, would reduce the value of the lift coefficient at a given incidence and Mach number, and hence would lead to a greater value of κ_i, the trend which is con-

trary to the observation that the values of κ_i obtained for the NACA 65_2-215 model are considerably smaller than those for the Model 70811 and the NACA 64A214 model.

Besides the incompleteness in the sealing of the side walls, it was already noted that some inaccuracy might be involved in the values of κ_i for the NACA 65_2-215 due to the separation of flow near the trailing edge. Again this inaccuracy would not be so serious that it could evoke such wide disparity in κ_i as was actually observed. Thus the only one remaining suspect is the boundary condition (4.4).

As was already remarked, a value of κ_i greater than unity indicates a negative value of P, which in turn implies a flow through the boundary in the direction reverse to the pressure gradient across it provided the assumption (2.9) is valid. For the moment let us assume that (2.9) holds approximately true.

Referring to Figs. 2 to 5, we see that a portion exists in the curve between $\Delta C_p(\fallingdotseq -2(u/U_\infty))$ and v along a perforated wall where P $(\fallingdotseq \Delta C_p/(2v/U_\infty))$ becomes negative. The existence of this portion is, according to Maeder (ref. 20), due to the turbulent mixing along a partly open boundary. In view of an evidence (ref. 31) that as far as the interference characteristics are concerned, a 20% open-area-ratio wall is effectively quite near to the open-jet boundary, it is very likely that this mixing effect does exist along part of the horizontal walls of the present 20% open-area-ratio test section.

If the relation between ΔC_p and v is such that the ratio $\Delta C_p/(v/U_\infty)$ is negative on the portion of the test-section walls which would exert greatest influence upon the flow field around the model, then the deduced value of κ_i would become greater than unity.

In short, we may claim that probably less inconsistent results would be obtained from an analysis made along the line of the present one if a proper account is taken of the fact that the curve of ΔC_p against v does not pass through the origin but that there is a portion on the curve where ΔC_p is negative while v is positive.

A possible way of realizing this supposition is to assume the boundary condition in the form

$$u+Kv=C \qquad (4.14)$$

instead of (2.5), where C is a *positive* constant which depends mainly on the structure of the perforated wall and the Mach number within the test section.

As for the assumption (2.9), we have scarce evidences with which to prove or disprove its validity. It is generally recognized that the static pressure in the plenum chamber away from the test-section walls is almost equal to the free-stream static pressure within the test section at the tunnel-empty condition. The static pressure in the plenum just outside the test section would not differ much from that far from the test-section walls, and the difference, if any, would not vary appreciably along the streamwise direction. Then the difference could be accounted for by choosing the value of the constant C in (4.14) appropriately.

The propriety of the form (4.14) and of the above conjecture about the validity of (2.9) can be attested by seeing whether the boundary condition (4.14) gives consistent prediction of the wall-interference characteristics with appropriate values of K and C, which can be determined from an analysis similar to the one taken in the present calculation.

V. CONCLUSIONS

(1) Analytical expressions of the wall-interference effects within a perforated wind tunnel were obtained for subsonic, two-dimensional cases based on a linearized-theory approach, which was reasoned to be of sufficient accuracy for the resolution of the interference effects on pressure distribution data.

(2) Combining the analytical results with the experimental data obtained on several aerofoil models, an attempt was made to determine the value of the porosity parameter for the 20% open-area-ratio test section of the NAL 2m×2m transonic wind tunnel from the condition that the theoretical value of the lift coefficient was to agree with the experimental one.

(3) Although the theoretical pressure distributions calculated using the value of the porosity parameter so determined were brought to close agreement with the experimental ones measured on the aerofoil models, it was found, on the one hand, that negative values of the parameter, which had been supposed to be always positive, were resulted in a few cases, and on the other, that there was a wide disparity among the values of the parameter obtained for several cases corresponding to different aerofoil models and to

different angles of attack for each of the models tested.

(4) Since the porosity parameter is thought to be only a function of the free-stream Mach number once one sticks to a particular test section, the disparity in its values derived from a variety of cases obviously indicates the failure of the approach taken thus far.

Possible causes of the failure were listed and examined, and the boundary condition in the theoretical model of the interference calculation was identified.

(5) An understanding of the genuine condition along a perforated wall was sought by consulting the literature on the experimental observations of the flow in the neighbourhood of the perforated-wall boundary.

As a result, it is suggested that the relation

$$u+Kv=C>0$$

will be more appropriate as the boundary condition than the

$$u+Kv=0$$

which has been adopted in the conventional theoretical model. Here C is a constant to be determined, just as with the coefficient K, from an experimental procedure for the particular test section one is concerned.

This renewed form of the boundary condition can explain, for instance, why the anomaly took place in some occasions that negative values were obtained for the porosity parameter with the conventional boundary condition.

ACKNOWLEDGEMENT

The experimental data on the NACA 65_2-215 and 64A214 models have become available to the author by courtesy of the Aerodynamic Group led by Mr. S. Kobayakawa of Nihon Aircraft Manufacturing Company, Ltd.

REFERENCES

1) R. C. Lock, B. J. Powell, C. C. L. Sells & P. G. Wilby: The Prediction of Aerofoil Pressure Distributions for Sub-critical Viscous Flows, AGARD C.P. No. 35, 1968.
2) Th. E. Labrujere, W. Loeve & J. W. Slooff: An Approximate Method for the Prediction of Pressure Distribution on Wings in the Lower Critical Speed Range, AGARD C.P. No. 35, 1968.
3) H. C. Garner, E. W. E. Rogers, W. A. E. Acum & E. C. Maskell: Subsonic Wind Tunnel Wall Corrections, AGARDograph No. 109, 1966.
4) B. H. Goethert: Transonic Wind Tunnel Testing, AGARDograph No. 49, 1961.
5) R. Brescia: Wall Interference in a Perforated Wind Tunnel, NACA TM 1429, 1957 (a translation of 'Studio dell'Interferenza delle Gallerie Aerodinamiche con Pareti a Fessure' published in Atti della Accademia delle Scienze di Torino, Vol. 87, 1952–1953).
6) D. D. Davis, Jr. & D. Moore: Analytical Study of Blockage- and Lift-interference corrections for Slotted Tunnels Obtained by the Substitution of an Equivalent Homogeneous Boundary for the Discrete Slots, NACA RM L53E07b, 1953.
7) B. S. Baldwin, J. B. Turner & E. D. Knechtel: Wall Interference in Wind Tunnels with Slotted and Porous Boundaries at Subsonic Speeds, NACA TN 3176, 1954.
8) L. C. Woods: On the Theory of Two-dimensional Wind Tunnels with Porous Walls, Proc. of the Royal Society, A. Vol. 233 pp.74–90, 1955.
9) L. C. Woods: On the Lifting Aerofoil in a Wind Tunnel with Porous Walls, Proc. of the Royal Society, A. Vol. 242 pp.341–354, 1957.
10) S. Katzoff & R. L. Barger: Boundary-induced Downwash Due to Lift in a Two-dimensional Slotted Wind Tunnel, NASA TR R-25, 1959.
11) R. H. Wright & R. L. Barger: Wind-tunnel Lift Intereference on Sweptback Wings in Rectangular Test Sections with Slotted Top and Bottom Walls, NASA TR R-241, 1966.
12) R. H. Wright & J. D. Keller: Wind-tunnel Lift Intereference on Sweptback Wings in Rectangular Test Sections with Slotted Side Walls, NASA TR R-344, 1970.
13) D. R. Holder: Upwash Interference in a Rectangular Wind Tunnel with Closed Side Walls and Porous-slotted Floor and Roof, A.R.C. R & M No. 3322, 1963.
14) D. R. Holder: Upwash Interference on Wings of Finite Span in a Rectangular Wind Tunnel with Closed Side Walls and Porous-slotted Floor and Roof, A.R.C. R & M No. 3395, 1965.
15) K. R. Rushton & Lucy M. Laing: A Digi-

tal Computer Solution of the Laplace Equation Using the Dynamic Relaxation Method, Aeronautical Quarterly Vol. XIX Part 4, 1968.

16) K. R. Rushton & Lucy M. Laing: A General Method of Studying Steady Lift Interference in Slotted and Perforated Tunnels, A.R.C. R & M No. 3567, 1969.

17) R. H. Wright & B. L. Schilling: Approximation of the Spanwise Distribution of Wind-tunnel-Boundary Interference on Lift of Wings in Rectangular Perforated-wall Test Sections, NASA TR R-285, 1968.

18) R. H. Wright & B. L. Schilling: Calculated Wind-tunnel-boundary Lift Interference Factors for Rectangular Perforated Test Sections, NASA TN D-5635, 1970.

19) E. M. de Jager & A. I. van de Vooren: Tunnel Wall Correctoins for a Wing-flap System between Two Parallel Walls, NLR TR W.7, 1965.

20) P. F. Maeder & H. U. Thommen: On the Boundary Layer at Perforated Walls, ZAMP Vol. IXb pp.438–453, 1958.

21) P. F. Maeder: Investigation of the Boundary Condition at a Perforated Wall, Tech. Rept. WT-9, Div. of Engineering, Brown Univ., 1953.

22) P. F. Maeder & A. D. Wood: Transonic Wind Tunnel Test Sections, ZAMP Vol.VII pp.177–212, 1956.

23) G. M. Stokes, D. D. Davis, Jr. & Th. B. Sellers: An Experimental Study of Porosity Characteristics of Perforated Materials in Normal and Parallel Flow, NACA TN 3085, 1954 (supercedes NACA RM L53H07, 1953).

24) C. F. Chen & J. W. Mears: Experimental and Theoretical Study of Mean Boundary Conditions at Perforated and Longitudinally Slotted Wind Tunnel Walls, Tech. Rept. WT-23, Div. of Engineering, Brown Univ., 1957.

25) P. F. Maeder & J. F. Hall: Investigation of Flow over Partially Open Wind Tunnel Walls, Tech. Rept. WT-19, Div. of Engineering, Brown Univ., 1955.

26) J. Lukasiewicz: Effects of Boundary Layer and Geometry on Characteristics of Perforated Walls for Transonic Wind Tunnels, Aerospace Engineering, Vol. 20, No. 4 p.22– 1961.

27) S. G. Mikhlin: Integral Equations, p.131, Pergamon Press, 1957.

28) R. C. Punkhurst & D. W. Holder: Wind-Tunnel Technique, Pitman & Sons, London, 1952.

29) NAL Staff: Design and Construction of the 2m×2m Transonic Wind Tunnel at the National Aeronautical Laboratory, NAL TR-25, 1962. (in Japanese)

30) S. Takanashi: A Method of Obtaining Transonic Shock-free Flow around Lifting Aerofoil Sections, to appear in the Transaction of the Japan Society for Aeronautical and Space Sciences.

31) J. R. Ongarato: Subsonic Wind Tunnel Wall Interference Studies Conducted in the North American Rockwell Corporation Trisonic Wind Tunnel, AIAA Paper No. 68–360, 1968.

32) M. Ebihara, Y. Ishida & T. Okonogi: A Description of Ideas Underlying a Computer Programme for Predicting Aerofoil Pressure Distributions in Subcritical Viscous Flow, NAL TR-248, 1971. (in Japanese)

Errata (TR 252T)

page	column	line	printed	should read
3	left	14	indeterminancy	indeterminacy
12	right	28	z_0	$\bar{z}_0$
15	right	33	c^2	c_2
17	left	13	Tus	Thus
17	left	21	x_c	x_p
19	left	4	potenal	potential

TR-247	On the theory of Free Streamlines Past an Arbitrary Shape	Hitoshi TAKAHASHI	Sep. 1971
TR-248	A Description of the Ideas Underlying a Computer Programme for Predictiag the Aerofoil Pressure Distributions in Subcritical Viscous Flow	Masao EBIHARA, Youji ISHIDA & Tokio OKONOGI	Nov. 1971
TR-249	Modified Optimization Algorithm for Computer Storage Problems in Generalized Newton-Raphson Method	Toru SHIHO	Oct. 1971
TR-250	Large Deflection of Cantilever Beams	Yasuo TADA & Kazuo HISAKA	Oct. 1971
TR-251	Inertial Force Field Due to Nutational Motion of Spinning Axi-symmetric Satellite and Its Application to Nutation Damper	Chikara MURAKAMI & Yoshiaki OHKAMI	Nov. 1971

TECHNICAL REPORT OF NATIONAL AEROSPACE LABORATORY
TR-252T

航空宇宙技術研究所報告 252T 号 (欧文)

昭和 47 年 1 月 発行

発行所 航空宇宙技術研究所
東京都調布市深大寺町 1,880
電話武蔵野三鷹(0422)47-5911(代表)

印刷所 株式会社 東京プレス
東京都板橋区桜川 2 丁目 27 の 12

Published by
NATIONAL AEROSPACE LABORATORY
1,880 Jindaiji, Chōfu, Tokyo
JAPAN